Srinil N, Ma B, Zhang L.

Experimental investigation on in-plane/out-of-plane vortex-induced vibrations of curved cylinder in parallel and perpendicular flows.

***Journal of Sound and Vibration* 2018, 421, 275-299.**

Experimental Investigation on In-plane/Out-of-Plane Vortex-Induced Vibrations of Curved Cylinder in Parallel and Perpendicular Flows

Narakorn Srinil*[a], Bowen Ma[a], Licong Zhang[b]

[a] School of Engineering, Marine, Offshore & Subsea Technology Group, Newcastle University, UK

[b] Department of Naval Architecture, Ocean & Marine Engineering, University of Strathclyde, UK

Abstract

This study is motivated by an industrial need to better understand the vortex-induced vibration (VIV) of a curved structure subject to current flows with varying directions whose data for model calibration and validation are lacking. In this paper, new experimental investigations on the two-degree-of-freedom in-plane/out-of-plane VIV of a rigid curved circular cylinder immersed in steady and uniform free-stream flows are presented. The principal objective is to examine how the approaching flow direction versus the cylinder curvature plane affects cross-flow and in-line VIV and the associated hydrodynamic properties. This is achieved by testing the curved cylinder in 3 different flow orientations comprising the parallel flows aligned with the curvature vertical plane in convex and concave configurations, and the flows perpendicular to the curvature plane. The case of varying flow velocities in a subcritical flow range with a maximum Reynolds number of about 50,000 is considered for the curved cylinder with a low mass ratio and damping ratio. Experimental results are presented and discussed in terms of the cylinder response amplitudes, inclination angles, mean displacements, motion trajectories, oscillation frequencies, hydrodynamic forces, relative phases, fluid excitation and added inertia coefficients. Comparisons with other experimental results of curved and straight cylinder VIV are also presented. The experiments highlight the important effects of cylinder curvature versus flow orientation on the combined cross-flow/in-line VIV. The maximum (minimum) responses occur in the perpendicular (convex) flow case whereas the extended lower-branch responses occur in the concave flow case. For perpendicular flows, some meaningful features are observed, including the appearances of cross-flow mean displacements and asymmetric eight-shaped motion trajectories due to multiple 2:1:1 resonances where two out-of-plane and one in-plane dominant frequencies are simultaneously excited. Overall VIV phenomena caused by the system asymmetry should be recognised in a prediction model and design codes to capture the combined effects of curved configuration and approaching flow direction.

Keywords: Vortex-induced vibration (VIV), fluid-structure interaction, experimental investigation, curved cylinder, two-degree-of-freedom oscillation

* Corresponding author: narakorn.srinil@newcastle.ac.uk; Tel. +44 191 208 6499; Fax +44 191 208 5491

Nomenclature

A_x/D (A_y/D)	Cylinder in-line (cross-flow) amplitude
C^*_x (C^*_y)	Coefficient of maximum in-line (cross-flow) total force
C'_x (C'_y)	Coefficient of root-mean-squared in-line (cross-flow) total force
C_{xm} (C_{ym})	Coefficient of mean in-line (cross-flow) total force
C_x (C_y)	Coefficient of time-varying in-line (cross-flow) total force
C^*_{vx} (C^*_{vy})	Coefficient of maximum in-line (cross-flow) force in phase with cylinder rotational velocity
C'_{vx} (C'_{vy})	Coefficient of root-mean-squared in-line (cross-flow) force in phase with cylinder rotational velocity
C^*_{ax} (C^*_{ay})	Coefficient of maximum in-line (cross-flow) force in phase with cylinder rotational acceleration
C'_{ax} (C'_{ay})	Coefficient of root-mean-squared in-line (cross-flow) force in phase with cylinder rotational acceleration
D	Curved cylinder external diameter (m)
I^*	Pendulum moment of inertia ratio (I/I_d)
I	Total moment of inertia about pivot point of pendulum and cylinder parts (kg.m^2)
I_d	Total moment of inertia about pivot point of displaced fluid (kg.m^2)
f_a	Natural frequency in air (Hz)
f_n	Cross-flow natural frequency in still water (Hz)
f_o	Oscillation frequency of cylinder or force response (Hz)
f_w	Natural frequency in still water (Hz)
L	Cylinder submerged length (m)
L/D	Aspect ratio based on cylinder submerged length
L_{hd}	Moment arm of fluid force from pivot point to cylinder neutral centre (m)
m^*	System mass ratio
m	System total mass contributing to cylinder oscillation (kg)
R	Curvature radius measured from cylinder axis (m)
Re	Reynolds number based on free-stream flow velocity
R/D	Cylinder radius ratio
t	Time in second (s)
V	Free stream flow velocity (m/s)
V_r	Reduced velocity parameter based on free stream flow velocity
X (Y)	In-line (cross-flow) direction with respect to flow orientation in Fig.1
x (y)	Cylinder time-varying in-line (cross-flow) response per diameter
$\overline{x}$	In-line mean displacement per diameter
$\overline{y}$	Cross-flow mean displacement per diameter
Z	Vertical direction in Fig. 1 based on right-hand rule
δ_y	Cylinder maximum global inclination angle from vertical axis and about pivot
ϕ_x, ϕ_y	Cylinder local inclination angle from the horizontal axis in Fig.1
θ_x, θ_y	Phase difference between force moment and cylinder rotational response
θ_{xy}	Phase difference between in-line and cross-flow responses
ξ_a	System damping ratio in air
ξ_w	System damping ratio in still water
ξ_{wy}	Cross-flow damping ratio in still water
ρ	Flow density (kg/m^3)

1. Introduction

Vortex-induced vibration (VIV) of a cylindrical structure immersed in fluid flows exhibits several fluid-elastic interaction phenomena depending on system parameters and resonance conditions. In offshore oil and gas applications, the effects of cyclic stress, fatigue and mean drag magnification caused by VIV are problematical for the lifecycle and integrity of underwater structures such as risers, pipelines, mooring lines, umbilical cables, tensioned legs, piles and fluid jumpers. Although several theoretical, numerical and experimental studies on VIV have been carried out over the past decades [1-5], relatively little is known about the effect of cylinder curvature in relation to the flow direction on the multi degree-of-freedom (DOF) VIV of a curved cylinder in a wide range of Reynolds number (Re), mass, damping and aspect ratios. From a practical viewpoint, a long rigid steel or flexible composite pipe such as a catenary or lazy-wave riser has a curved portion influenced by the weight, buoyancy and current mean drag force. A certain curvature plane constitutes an initial reference configuration of the curved cylinder subject to incoming flows [6]. As VIV takes place, the associated dynamics can be categorised, with respect to the curvature plane, as in-plane and out-of-plane responses depending on the flow direction [7-9]. Despite the practical importance of curved structures, experimental data of curved cylinder VIV which can be useful for model calibration and validation are still lacking in the literature, in comparison with data of straight cylinder VIV. In this study, new experimental investigations on the 2-DOF VIV of rigid curved circular cylinders subject to parallel (concave/convex) and perpendicular flows are presented, providing new insights into the associated fluid-structure interaction behaviours.

For stationary rigid curved cylinders, a few researchers have carried out the computational fluid dynamics (CFD) analysis to understand fundamental features of the spatial vortex shedding and three-dimensional wake dynamics. Miliou et al. [10] considered a quarter-ring cylinder with a constant curvature radius R (measured through the cylinder axis) per the outer diameter (D) R/D = 12.5. In the perpendicular flow case at Re = 100, they found that the cylinder wake behaves similarly to that of a vertical cylinder, by having a single dominant vortex-shedding frequency in the lift forces. Nevertheless, due to unequal strengths of the two shedding vortices, a mean cross-flow force component was noticed alongside a mean drag force whereas the oscillating in-line force exhibited two dominant frequencies. With the same R/D = 12.5, Miliou et al. [11] considered convex/concave flows at Re = 100 and 500, by also accounting for a horizontal extension part of 10D for the convex cylinder and a vertical extension part of 6D for the concave cylinder. Their CFD results highlighted the key role of axial velocity component and the increasing Re effect on the wake instabilities. For the convex geometry, a single dominant vortex-shedding frequency was found to dominate the entire cylinder span: this suggests the independence of local Re variation. For the concave geometry, the vortex shedding was found to be suppressed and the total drag force was weakened by strong axial flow components. The axial flows became strengthened at higher Re, partially suppressing the vortex shedding generated by the vertical straight section. Recently, Gallardo et al. [12] performed direct numerical simulations of flow past a convex cylinder with R/D=12.5 at higher Re = 3900 to investigate the turbulent wake features. Their curved cylinder also had a horizontal and vertical extension of 10D and 6D, respectively. Results

revealed two distinctive upper and lower wake regions separated by a location at an inclination angle of about 45°, with the former revealing a regular vortex shedding whereas the latter showing a less vigorous vortex strength due to the enhanced three-dimensionality and coherence loss of flows. At a higher Re = 1.5×10^5, Xu and Cater [13] performed a CFD study on both convex and concave cylinders with R/D = 12.5 and a vertical extension of 20D. They concluded that the concave flow case is superior to the convex one due to the suppression of vortices and lower drag/lift forces in the former.

Nevertheless, the wake characteristics in the case of oscillating cylinders become quite distinctive from the above-mentioned features in the case of stationary cylinders. de Vecchi et al. [14] extended the work of Miliou et al. [11] to account for the influence of cylinder forced motion on the near-wake dynamics, force distributions and fluid-body energy transfer. A harmonic out-of-plane motion with a specified amplitude and frequency around a Strouhal value was implemented for both convex and concave cylinders with R/D = 12.5 and Re = 100. In the convex case subject to a forced translation, a strong correlation of vortices with in-phase vortex-shedding along the span was noticed. However, the horizontal extension of 10D produced a strong hydrodynamic damping to the system leading to a lack of positive energy transfer from the fluid to the cylinder. By imposing a forced rotation about the horizontal extension, such damping mechanism was inhibited due to the out-of-phase vortex shedding leading to the non-uniform lift force distribution. In the concave configuration, the forced transverse motion was found to trigger a positive fluid energy transfer. This excitation mechanism is distinctive from the associated stationary concave cylinder where axial flows produce the stabilising mechanism of the vortex shedding [11]. Further, de Vecchi et al. [15] studied the effect of varying amplitudes and frequencies of the forced transverse motions on the wake dynamics of the convex cylinder. Their numerical results suggest a strong dependence of the fluid-structure energy transfer mechanism on the cylinder motion combined with the cylinder curvature effect.

For freely oscillating curved cylinders, Assi et al. [16] investigated the 2-DOF VIV of a low mass and damping cylinder in both convex and concave configurations with R/D = 10 and in the Re range of 750-15000. They found that, in comparison with a vertical cylinder VIV, both out-of-plane (cross-flow) and in-plane (in-line) maximum amplitudes of curved cylinders are reduced due to the curvature effect. The concave cylinder exhibited the sustained responses beyond the main synchronisation range. With the flow visualisation on a stationary curved cylinder at Re = 1000, such feature could be generated by another fluid-instability mechanism associated with the wake interference of the horizontal section located upstream. The decreased response due to the curvature effect was also observed by Seyed-Aghazadeh et al. [17] who conducted a 1-DOF VIV experiment of convex/concave cylinders with R/D = 47 in a lower Re range of 300-2300. The extended cross-flow response was also reported in the concave case. Nevertheless, the in-line VIV effect was not accounted for in their studies.

Table 1 summarises relevant models of rigid curved stationary/oscillating cylinders and associated flow orientations based on the above-reviewed papers. The comparison reveals their different flow-cylinder properties including R/D, Re, the cylinder extension sections and motion status. Only one paper has considered a 1-DOF or 2-DOF free vibration, and a perpendicular flow case for a stationary cylinder.

Therefore, there is a lack of research in the 2-DOF VIV of curved rigid cylinders in perpendicular versus parallel flows. These aspects will be experimentally investigated and discussed in this study.

This paper is structured as follows. In Section 2, a free-vibration experimental model for the study on 2-DOF VIV of a rigid curved circular cylinder in steady and uniform flows is presented. Cylinder cross-flow and in-line (out-of-plane or in-plane) responses, inclination angles, motion trajectories, mean displacements and oscillation frequencies are reported in Section 3. The system phase differences and hydrodynamic coefficients of the fluid forces in phase with the cylinder velocities and accelerations are presented in Section 4. The obtained experimental results are also compared with other VIV tests of curved/straight cylinders, and discussed with some observations from previous numerical simulations of flows past stationary/oscillating curved cylinders. The paper ends with the conclusions in Section 5 and a theoretical formulation for estimating the hydrodynamic properties in the Appendix.

It is worth emphasizing that actual motivation of this experimental study lies in the understanding of the potential asymmetry effect, arising from the approaching flow orientation versus the cylinder curvature plane in convex/concave and perpendicular configurations, on the combined cross-flow/in-line VIV, the mean displacements and the associated hydrodynamic properties in a subcritical flow range with the maximum Re ≈ 50,000. Even though a small scale model with specific geometries are considered, the ensuing experimental data and observations may be meaningful for comparisons of VIV behaviours with a practical larger-scale model with fixed/variable curvatures and flow directions. Apart from capturing actual physical insights, the present experimental response and hydrodynamic data could be useful for calibration and modification of empirical coefficients in the phenomenological reduced-order models [6-8, 18-20] as well as for the current industry practice of using a strip-theory approach.

2. Experimental Setup

An experimental rig for the study of 2-DOF VIV of an elastically mounted rigid cylinder subject to uniform and steady flows has been developed in a towing tank at the Kelvin Hydrodynamics Laboratory in Glasgow [21]. Previous VIV results of vertical straight cylinders have been validated by those from other tests [22, 23] and by numerical predictions [19]. The towing tank has a dimension of 76 m long by 4.57 m wide with the water depth in the range of 0.5-2.3 m. It is equipped with a self-propelled towing carriage on which the apparatus can be firmly installed and with a variety of damping systems to calm the water rapidly between runs. In the present study, this 2-DOF test rig is used for new experiments of a rigid curved circular cylinder to investigate the effect of cylinder curvature versus the approaching flow direction in convex, concave and perpendicular flows.

Figure 1 displays the experimental arrangement where the submerged curved cylinder is vertically mounted and connected at its upper end to a long composite pendulum made of aluminium (upper part) and carbon fibre (lower part). The aluminium part has a length of about 15.5D whereas the carbon fibre part with a small 50mm submergence has a length of about 21.7D where D is the curved cylinder external diameter of about 11 cm. The pendulum is pivoted at the top of supporting frames through a high-precision universal joint allowing free rotations. The use of carbon fibre with a low material

density is recommended to ensure a system low mass ratio m^* ($m^* = 4m/\rho\pi D^2 L$, where m is the system total mass contributing to the oscillation, ρ the flow density and L the cylinder total submerged length). The curved cylinder is made of the Polyvinyl Chloride Polymer (model D281) tube; it is uniformly filled with small lead balls such that $m^* \approx 1.9$. This $m^* < 6$ promotes greater in-line and cross-flow VIV [24], being of practical interest in offshore applications. The curved cylinder is fully submerged and has two main parts consisting of a quarter ring with $R/D = 5$ and a truncated horizontal section with a length of 3D. These make the aspect ratio (L/D) of the total submerged cylinder (i.e. the vertical submergence of 50mm plus the quarter ring and horizontal extension parts) of about 11 which is comparable to L/D in other tests [24-27]. The horizontal extension is also considered to examine whether there is a potential wake-induced instability [16] or damping effect [11] in the concave and convex cases, respectively. However, the limited horizontal length of 3D is considered to avoid the cylinder torsional or upward bending oscillation during the towing. All components of the pendulum are firmly connected to maximise the system integrity during the towing test runs.

Note that offshore risers, flowlines, pipelines, jumpers and j-tubes are practically installed in a variety of configurations depending on, e.g., the water depth, environment, support fixed/floating platform and material flexibility, and they establish a curved portion with a fixed or variable bend radius [7, 28-30]. For a so-called rigid pipeline-riser system applied to a fixed jacket platform, the typical value of the minimum bend radius (MBR) of the curved portion is about 3D-5D [31]. For a flexible riser forming a catenary, S or lazy-wave shape and connecting a floater in deep waters, the fixed (static) MBR is about 5.5D-7D whereas the variable (dynamic) MBR is about 8D-12D [32]. For a steel-made catenary riser, the MBR is 25 times higher than the above ranges of flexible riser [32]. For a rigid M-shaped subsea jumper, the MBR is about 3D-5D [33]. Hence, our experimental model of a quarter-ring cylinder with a fixed bend radius of 5D is applicable to a curved portion of the rigid pipeline-riser configuration and the subsea jumper, apart from potentially representing a flexible riser curved portion as the limiting case.

By using two pairs of coil springs rearranged perpendicularly in the horizontal plane as in Fig. 1, the mechanical system enables the cylinder to freely oscillate with arbitrary in-plane and out-of-plane responses either in the in-line (X) or cross-flow (Y) direction, depending on the incoming flow (X) direction. Each spring obeys the Hooke's law and has a constant linear stiffness. Measurement of cylinder motions is carried out by using a Qualisys optical motion capture system with a fixed sampling frequency of 137 Hz. This non-contact system prevents the unwanted damping or restoring forces from influencing the mechanical system. Four infrared cameras are used to identify and optimise the multi positions of the very light reflective markers mounted on the pendulum. Calibration is performed with an average residual across all cameras of less than 0.3 mm. Key outputs are rotational angles with a resolution of 10^{-3}. The time-varying spring forces are also measured via two-dimensional pairs of calibrated load cells with a maximum load capacity of 500 N and a resolution of 10^{-4}. These spring forces will be used in the estimation of hydrodynamic properties as in the Appendix. The acquisition time for a steady-state response is about 2 min and the waiting time between each two consecutive runs

is about 5-10 min, dependent on the towing speed. A trailing wheel of accurately defined circumference is attached to the carriage, and the wheel angular velocity is determined using a high-precision magnetic encoder and a counter-time which outputs the velocity signal signifying the carriage speed (less than 1% of fluctuation throughout the run) and thus the free stream flow velocity V [21]. Any noise or high frequencies of the frames are filtered out by using the inverse Fast Fourier Transform (FFT). Other challenges associated with the towed cylinder setup are discussed below.

- *Free surface effect*: The starting point of the curved cylinder is located about 50 mm beneath the static free surface. Thus, there is a very little immersion of the main vertical cylinder section in the water. During the towing, no appreciable surface disturbance or piercing was visible due to a horizontal spring-based constraint. With a similar pendulum arrangement, Assi et al. [16] have shown the negligible effect of varying the vertical extension length (from 0-10D) on the 2-DOF VIV of curved cylinders. Also, Goncalves et al. [34] have suggested that the free surface effect would become important for the cylinder with $L/D < 5$ which is lower than $L/D = 11$ considered in this study.
- *Rotational pendulum effect*: The rotating pendulum effect on the uniformity of local flow fields is deduced to be negligible since the maximum global inclination angles (inclusive of mean values) of the cylinder measured vertically about the pivot point from the Z axis are found to be less than 15^o in all tests. Franzini et al. [27] showed that the effect of cylinder inclination of being less than 20^o on 2-DOF VIV might be negligible. With the pendulum arrangement, a cylinder vertical upward motion could be induced by axial or tangential flow components [11, 12]. However, this is considered to be also negligible due to such small rotational angles.
- *Blockage effect*: The blockage may be considered as a ratio of the stationary cylinder projection width to the tank cross-flow width. In this study, the blockage is about 2.5% in the parallel flow cases whereas it is increased due to the horizontal extension to about 8.4% in the perpendicular flow case. Depending on m^*, ξ, Re, flow turbulence and disturbance, the blockage may affect the onset of lock-in and maximum VIV response. Nevertheless, the present study has a maximum blockage similar to that of 8.3%, 8.4%, 10% and 8.3% reported by some well-known VIV tests of straight cylinders in Feng [35], Bishop and Hassan [36], Khalak and Williamson [37], and [38], respectively.
- *Bottom proximity effect*: The lowest horizontal part of the curved cylinder is located about 10D from the tank bottom. Such a proximity condition or gap ratio is deemed to produce a negligible effect on VIV responses for the considered subcritical flows with Re of order 10^4 [36, 39-41].

Prior to the towing experiments, free decay tests in air and in still water were performed to identify natural frequencies and damping of the pendulum system in both in-plane and out-of-plane directions. Repeated tests were considered and the variability in the free-vibration results was found to be less than 2%. Table 2 lists properties of the present 2-DOF curved cylinder model with m^*, ξ_a (ξ_w) the damping ratio in air (in water), f_a (f_w) the natural frequency in air (in still water), in comparison with those of the 2-DOF curved cylinder model of Assi et al. [16]. The present apparatus was found to be lightly damped with the averaged $\xi_a < 1\%$ and $\xi_w < 2.5\%$; having slightly unequal damping between in-plane and out-of-plane directions. The in-plane-to-out-of-plane natural frequency ratio is about 1.03 in air and 1.17 in

water. These two-directionally distinctive damping and frequency values reflect the effect of cylinder curved geometry and additional fluid-added damping [42]. Depending on the cylinder orientation and flow direction, the cross-flow (in-plane or out-of-plane) natural frequency in still water (f_n) will be used in forming the reduced velocity parameter ($V_r = V/f_nD$) where V is varied to capture the variation of cylinder VIV responses, hydrodynamic properties and their maximum components.

3. Experimental Results and Discussion

Experimental tests have been carried out for convex, concave and perpendicular flows. As the flow direction (X) is aligned with, but opposite to, the towing direction, three global coordinate systems for different cylinder orientations are introduced in Fig. 1 (a-c) based on a right-hand rule so that Y axis corresponds to cross-flow VIV whereas X axis corresponds to in-line VIV. Based on the measured angles, cross-flow (A_y/D) and in-line (A_x/D) amplitudes normalised by the cylinder diameter are evaluated by referring to the displacements at an intersection point between the two central lines of the cylinder vertical and horizontal parts (i.e. point C in Fig. 1). In the following, experimental results of cylinder amplitudes, inclination angles, their mean components, two-dimensional motion trajectories and oscillation frequencies are reported and discussed whereas the associated hydrodynamic properties are presented in Section 4.

3.1 Cross-Flow and In-Line Amplitudes

Figure 2 presents comparisons of A_y/D and A_x/D in concave and convex flow cases with results of [16] whose the curved cylinder without the submerged vertical extension is considered. For concave flows, the present cylinder with the lower m^* =1.9 exhibits a response jump from an initial branch to the upper branch at $V_r \approx 5$, achieving a greater maximum $A_y/D \approx 1.1$ (Fig. 2a) and $A_x/D \approx 0.2$ (Fig. 2c) at $V_r \approx 8$. This jump has been verified by performing several repeated tests around that V_r. Similar to the tests in [16], the present concave cylinder shows a sustained lower-branch A_y/D response which takes place beyond the main lock-in range (V_r >10). Such response extension may be attributed to the effect of wake-induced instability generated from the leading horizontal part against the incoming flow which leads to the energy transfer from the fluid to the structure [14]. For convex flows, the maximum $A_y/D \approx$ 0.6 (Fig. 2b) and $0.07<A_x/D<0.09$ (Fig. 2d) are comparable in both tests with similar m^* and ξ_a. However, the convex flow case does not show the extended lock-in range and its single-peak diagram is similar to that of a straight cylinder VIV, with the main lock-in range of about $4<V_r<10$. This feature may be linked to the CFD study on a stationary convex cylinder where the wake vortex shedding in the upper curved body drives the lower end at a single dominant shedding frequency for the whole curved span [11]. As the pressure centre of the curved portion is located downstream of the vertical pendulum, the hydrodynamic damping might be generated, stabilising the cylinder responses [14-16].

Overall, considerable differences in both A_y/D and A_x/D are noticed in the concave case, and this may be attributed to the combined differences in the horizontal (3D vs. 10D) and vertical (0.45D vs. 0) extension lengths of the submerged cylinders (Table 1), m^*, ξ (Table 2) and experimental setup such as the effect of pendulum length, inclination angle, and the use of water flume in [16] versus towing tank

in this study. Nevertheless, both studies show overall greater 2-DOF VIV responses in concave flow cases than those in convex flow cases.

Comparisons of A_x/D and A_y/D based on the present convex, concave and perpendicular flow tests are now presented in Figs. 3a and 3b, respectively. It can be remarked that the perpendicular case produces the greatest responses with maximum $A_x/D \approx 0.38$ and $A_y/D \approx 1.85$. Also, this case reveals a small pure in-line VIV at $V_r \approx 2$ (Fig. 3a) and a cross-flow response jump from its upper branch to the lower one at $V_r \approx 10$ (Fig. 3b). This jump behaviour, which is typically observed in a 2-DOF VIV test of straight cylinders with a low m^*, is associated with the hysteresis phenomenon depending on initial conditions [41]. With these observations, both A_x/D (Fig. 3c) and A_y/D (Fig. 3d) results in the perpendicular flows are also compared with those from the straight cylinder tests with $m^* = 2.6$ [24] and $m^* = 2.8$ [16]. Similar 2-DOF VIV features with initial, upper and lower branches between $4< V_r <12$ can be seen with comparable A_x/D and A_y/D. Geometrically speaking, this qualitative similarity might be due to the local flow velocity being spatially perpendicular to the cylinder vertical as well as horizontal axes. This minimises the occurrence of axial flow components which can disrupt the vortex shedding correlation along the curved span [11, 12].

3.2 Mean and Oscillation Inclination Angles

For flow around inclined or yawed circular cylinders, the most common approach is to refer to the independence principle which states that the flow characteristics and VIV response may depend on the local flow velocity component normal to the cylinder axis [43-45]. Based on experimental studies on stationary inclined cylinders, van Atta [46] reported that the independence principle is valid for inclination angles up to about 35^o whereas Snarski [47] suggested that the flow regime remains similar to the classical vortex shedding pattern for angles up to about 37^o. Using 3-D numerical simulations, Zhao et al. [48] have recently shown the independence principle validity in terms of the hydrodynamic properties for angles up to about 30^o. Within this inclination range, the vortex shedding wake is kept parallel to the cylinder axis. This feature has also been highlighted in [11] and [12] for a stationary rigid curved cylinder in convex flows. Recently, for 2-DOF VIV of inclined cylinders, Franzini et al. [27] have experimentally investigated the effects of upstream and downstream inclinations, and suggested how the independence principle might be valid for inclination angles less than $\pm 20^0$.

With reference to Fig. 1, a local inclination angle (ϕ) of the curved cylinder part is evaluated, which is measured from the horizontal axis (i.e. X in the parallel flow case and Y in the perpendicular flow case) to the tangential line of the curved cylinder axis. Two reference points A and B are considered, representing the starting and ending points of the curved cylinder. Prior to the oscillation, point A has $\phi = 90^o$ whereas point B has $\phi = 0^o$. Along the curved cylinder, ϕ is thus varied from 90^o to 0^o according to the rigid curved geometry. Due to the effects of mean drag and VIV, such initial static ϕ angles are further modified depending on the flow-cylinder orientation.

Figure 4 illustrates the time-varying in-line (ϕ_x) and cross-flow (ϕ_y) local inclination angles (inclusive initial, mean and oscillation components) at points A and B associated with the maximum

VIV responses in Figs. 3a and 3b for convex (4a, 4b), concave (4c, 4d) and perpendicular (4e and 4f) flow cases. Some observations can be remarked. First, there is a small modification of the static angles (90^o or 0^o) due to the mean drag force components, and this is clearly seen for in-line VIV in planar flow cases (4a, 4b, 4c and 4d). The modification of cross-flow mean angles is negligible (4e and 4f) due to the negligible mean lift forces. For in-line VIV, the maximum change in ϕ_x is by about 0.5^o in the convex flow case and 1^o in the concave flow case. For cross-flow VIV in the perpendicular flow case, the maximum change in ϕ_y is by about 2.5^o due to the fluctuation of oscillation angle components.

By combining the mean and oscillation components, Fig. 5 presents the maximum ϕ_x in convex (Figs. 5a and 5b) and concave (Figs. 5c and 5d) flow cases and the maximum ϕ_y in perpendicular flow cases (Figs. 5e and 5f), at points A and B. Overall results highlight the V_r dependence and the flow orientation effect. For planar flows, ϕ_x at point A (B) decreases (increases) with V_r due to the increased drag force effect, with the overall maximum change in ϕ_x of about 2^o in the concave case. As the mean lift components are negligible for perpendicular flows, the ϕ_y diagrams exhibit similar features to the associated amplitude responses (Fig. 3b) with a maximum change in ϕ_y of about 2.5^o at $V_r \approx 9$ followed by a response jump. The local inclination plots in Figs. 4 and 5 allow us to recognise how the local flow velocities may be decomposed into the normal ($\sin\phi$) and tangential ($\cos\phi$) components along the curved cylinder according to the independence principle. Accordingly, the effective reduced flow velocity, based on the normal flow component, changes along the curved cylinder length [11, 12].

With reference to point C in Fig. 1, the maximum global inclination angle (measured vertically from the Z axis about the pivot) in the cross-flow direction δ_y and in the perpendicular flow case are plotted in Fig. 6 (based on the oscillation components) and compared with previous 2-DOF VIV results of the pivoted straight cylinders [49-51]. Results are based on different moment of inertia ratios I^* ($I^*=I/I_d$ where I is the structural inertia and I_d is the displaced fluid inertia about the pivot point). Key parameters of different test setups are also compared in Table 3. Note that if the pivoted cylinder is fully submerged, $I^* = m^*$. It can be seen that the maximum $\delta_y < 0.05$ rad ($\approx 3^o$) which justifies the nearly uniform free stream condition in the present study. The test setups with low ξ_{wy} (1-3%) provide similar maximum δ_y values ($\approx$ 0.02-0.05) and the lock-in range increasing with decreasing m^*. Quantitative differences are still noticed which are attributed to the VIV dependence on several individual parameters (m^*,ξ_w, I^*, Re) and experimental setups.

3.3 Appearance of Cross-Flow Mean Displacements

For 2-DOF VIV of straight cylinders, it is well known that the mean in-line or drag force generally increases with V and it can be further amplified by VIV responses within the main lock-in range [26]. For sub-critical flows with $Re < 3x10^5$ [41], a cross-flow mean force is typically not observed due to the geometry symmetry leading to a pair of equal-strength vortices being shed per the lift cycle. In a critical flow regime with $3x10^5 < Re < 3.5x10^5$ [52], the non-zero cross-flow mean force has been observed when the boundary layer separation is turbulent at one side of the cylinder. Nevertheless, this is not the case for the curved cylinder with the geometry asymmetry in sub-critical flows. As highlighted

in Fig. 7, there are some non-trivial cross-flow mean drifts per cylinder diameter $\overline{y}$ (Fig. 7c), in addition to the in-line ones $\overline{x}$ (Fig. 7a), in all curved cylinder cases. In association with the maximum amplitudes (Figs. 3a and 3b), both $\overline{x}$ and $\overline{y}$ in the perpendicular flow case become the greatest around $V_r \approx 8$ and exhibit a visible response jump. This free-oscillation behaviour may be linked to the CFD studies where numerical simulations revealed the occurrence of cross-flow mean components with the perpendicular [10] and convex [12] flows past a stationary curved cylinder. Although the maximum $\overline{y} \approx 0.1$ is much lower than the associated maximum $\overline{x} \approx 1.8$ in the present study, such $\overline{y}$ appearance might become more pronounced for a curved cylinder with a greater *R/D*, *L/D* or Re.

For a specific $V_r \approx 8$, the normalised in-line (out-of-plane) and cross-flow (in-plane) response time histories in the perpendicular flow case are exemplified in Figs. 7b and 7d, respectively. Besides the initial transients, the steady-state 2-DOF drift features are illustrated with a greater fluctuation in the in-line response. The associated mean force coefficients will be discussed in Section 4. Herein, it is worth remarking that the mean-valued displacements will have a direct impact on a practical design of curved cylindrical structures as these static deformations can modify the restoring forces, change the structural natural frequencies and subsequently the onsets of multi-directional lock-in resonances.

3.4 Dual and Multiple Resonances

It is of practical importance to understand the resonance conditions of curved cylinder VIV in different flow orientations. Accordingly, the two-dimensional in-plane/out-of-plane trajectories of cylinder motions and hydrodynamic forces with about 10 periods of the associated cross-flow oscillation frequencies are displayed in Figs. 8a and 8b, respectively. The *x*-*y* phase differences of responses and hydrodynamic forces are defined as in the Appendix, and the associated results will be discussed alongside the relative phases between the forces and motions in Section 4. In addition to the *x*-*y* trajectories, frequency spectra based on the FFT analysis are presented in Figs. 9 and 10 to identify the system oscillation frequencies (f_o). Note that the vertical axis labels in Figs. 9a-9d are set differently from those in Figs. 9e-9f to increase the frequency peak visibility in the former case.

It can be seen in Fig. 8a that the majority of cylinder trajectories exhibit the figure-of-eight patterns with two lobs pointing downstream. These features are associated with dual resonances [20, 53] with predominant 2:1 oscillation frequency ratios between in-line and cross-flow responses as displayed in Fig. 9. These dual resonances are more noticeable in the perpendicular (Figs. 9e and 9f) and concave (Figs. 9c and 9d) flow cases than in the convex flow case (Figs. 9a and 9b) owing to smaller in-line responses of the latter (Fig. 3a). In the wake-induced vibration range ($V_r > 10$) with sustained A_y/D in the concave case (Fig. 3b), the eight-shaped feature disappears since the associated A_x/D are quite small, fluctuating in time (e.g. Fig. 7b). These results are qualitatively similar to those reported in [16] for the curved cylinder test in a water flume. Overall, some amplitude modulations are visible in Fig. 8a with non-repeatable trajectories around the main lock-in region. These are typically observed in the 2-DOF VIV experiments due to strong fluid-cylinder interactions [21, 53]. The cylinder 2:1 resonances occur despite initially having the still-water *X*-*Y* natural frequency ratio of about 1.17 (Table 2). This suggests

the modification of hydrodynamic added mass due to VIV [20, 53] as presented in Section 4.

As for the *X*-*Y* force trajectories depicted in Fig. 8b, the appearances of figure-of-eight patterns are in accordance with those *X*-*Y* cylinder motions in Fig. 8a, in each flow orientation. Nevertheless, for large-amplitude responses in the perpendicular case, some asymmetry features are remarkable in both the force (Fig. 8b) and cylinder (Fig. 8a) trajectories and these are due to the presence of other harmonics. By inspecting through Figs. 9e and 10e in the perpendicular case, there is a secondary lower-frequency (about a half of the main frequency) peak in both cylinder and force in-line (out-of-plane) responses in a particular V_r range. Such frequency corresponds to that of the coexisting cross-flow (in-plane) response (Figs. 9f and 10f). This feature of two coexisting in-line oscillation frequencies, leading to a multiple 2:1:1 resonance and asymmetric figure-of-eight trajectory, distinguishes the curved cylinder in perpendicular flow from that in concave and convex flows. This multiple resonance has also been observed in 2-DOF VIV of rigid straight cylinders with in-line to cross-flow natural frequency ratios close to 1:1 [54, 55]. Results in Figs. 9f and 10f experimentally exhibit features similar to what has been observed by numerical simulations of perpendicular flows past a stationary curved cylinder [10] where two dominant oscillation frequencies in an in-line force response were observed as a result of unequal strengths of the alternate vortex shedding. Herein, by allowing the cylinder to oscillate, the 2:1 in-line frequencies are locked-in with the cylinder motion in addition to the cross-flow resonance. A multiple resonance in VIV of a flexible catenary has also been captured through a prediction model of Srinil [6].

In Fig. 10, it can be noticed from the FFT plots that cross-flow force amplitudes (Figs. 10b and 10d) are much greater than the associated in-line ones (Figs. 10a and 10c) in parallel flow cases. However, the in-line forces are substantially increased, becoming comparable to the cross-flow forces in the perpendicular flow case (Fig. 10e vs. 10f). This gives rise to the enhanced fluid-structure interactions and therefore greater *X*-*Y* responses (Figs. 3 and 8).

Figure 11 plots the cylinder and force oscillation frequencies normalised by the associated still-water cross-flow natural frequencies (f_o/f_n) for convex (Fig. 11a), concave (Fig. 11b) and perpendicular (Fig. 11c) flow cases. Two inclined dashed lines with different slopes are also given to represent the Strouhal number of 0.2 and 0.4 associated with cross-flow and in-line vortex shedding frequencies, respectively, for a smooth stationary circular cylinder in subcritical flows [42]. It can be seen in Figs. 11a-11c that f_o/f_n values in both directions follow the Strouhal trends at low V around the beginning of the upper branch ($V_r \approx 4$) and, thereafter, f_o/f_n values noticeably deviate from the slope lines due to a lock-in condition [41]. In association with Figs. 8 to 10, the ratios of f_o/f_n between in-line and cross-flow responses are within $2 \pm 20\%$ in the synchronization range of $4< V_r <10$. This justifies their nearly 2:1 resonances in all curved cylinder cases. In the lock-out range ($V_r >10$) where in-line responses are small, randomness in frequencies is realised and the associated f_o/f_n data are much scattered especially in the convex case. This observation in oscillation frequencies is in agreement with results of [16].

In addition to the primary peaks of 2:1 resonances, the secondary in-line oscillation frequencies – being comparable to the cross-flow oscillation frequencies – are only observed in the perpendicular flow case (Figs. 9e, 9f, 10e and 10f). Their f_o/f_n ratios are plotted in Fig. 11d which justifies the multiple

2:1:1 (inline:in-line:cross-flow or out-of-plane:out-of-plane:in-plane) resonances and asymmetric 8-shaped trajectories (Fig. 8) in the $6< V_r <10$ range. Figure 12 illustrates the in-line response time histories which exhibit the multiple peaks resulting from the 2:1 oscillation frequencies for the selected V_r = 6.02, 6.74, 7.14 and 8.04. The amplitude modulation features also suggest that the RMS responses cannot be simply computed by assuming a single harmonic motion (i.e., $A_{xRMS}/D \neq (1/\sqrt{2})A_x/D$).

4. Hydrodynamic Characteristics

It is of theoretical and practical interest to evaluate the hydrodynamic properties of the present fluid-structure interaction system of curved cylinder undergoing in-plane and out-of-plane VIV based on the measured responses and forces. In so doing, the equations of dynamic angular momenta governing the pivoted cylinder coupled with the horizontal springs are derived as described in the Appendix. The system relative phases, hydrodynamic forces and coefficients are approximated, by also distinguishing the forces in phase with the cylinder rotational accelerations and velocities, based on the obtained added moment of inertia and added rotational excitation. Note that, although the actual centre of the space-time varying resultant fluid force is unknown, it is feasible to define the hydrodynamic properties by referring to a particular position from the pivot point. In this study, the neutral point of the submerged body parts is considered, providing the moment arm of the hydrodynamic force from the pivot point in each direction (L_{hd} in Eq. A.7 and A.8 in the Appendix).

With varying V_r, Fig. 13 plots the time-averaged relative phases (θ_x, θ_y), normalised with π, between the fluid forces and cylinder responses in each in-line (Fig. 13a) and cross-flow (Fig. 13b) direction for convex, concave and perpendicular flows. The hydrodynamic excitation force is associated with $0<\theta/\pi \leq 1$, according to the assumed solution in Eq. A.10 regarding the force in-phase with the cylinder velocity. In association with the response amplitudes in Figs. 3a and 3b, Figs. 13a and 13b highlight that the curved cylinder is excited by the vortex-induced forces in all flow configuration cases. For parallel flows, the convex cylinder illustrates $0.25<\theta/\pi < 1$ for the main excitation range ($4<V_r<10$) whereas the concave cylinder illustrates $0.25<\theta/\pi < 0.75$ for the wider excitation range ($4<V_r<16$). In the latter case, it is noticed that both θ_x/π and θ_y/π remain nearly a constant of about 0.75 associated with the sustained large cross-flow response shown in Fig. 3b. For perpendicular flows which result in the largest responses, the main excitation range ($4<V_r<10$) exhibits the broadest range of $0<\theta/\pi < 1$ as well as a jump in θ_y/π from being about 0.5 to 0.75 at $V_r \approx 10$. This phase jump is associated with a response transition (Fig. 3b) from the supper-upper branch to the lower branch for the 2-DOF VIV [24].

Corresponding to the *x*-*y* motion and force trajectories in Fig. 8, the time-averaged, normalised θ_{xy}/π values are plotted in Fig. 13c. By following the motion of the trajectory's top part [53], counter-clockwise ($1.5<\theta_{xy}/\pi<2$) and clockwise ($0.5<\theta_{xy}/\pi<1.5$) trajectories may be identified as in [24] based on the same θ_{xy} definition, depending on the flow orientation and V_r. Near the peak ($V_r \approx 10$) and within the lower-branch responses ($V_r >10$; see also Fig. 3b), the perpendicular flow case exhibits the counter-clockwise orbits which are qualitatively similar to what have been experimentally observed in Dahl [54] for 2-DOF VIV of straight cylinders. On the contrary, both concave and convex flow cases reveal the

majority of clockwise trajectories, except for V_r >10 where the concave flow shows the counter-clockwise ones associated with the sustained *y* responses presented in Fig. 3b.

Figure 14 presents the excitation coefficients (C'_{vx}, C'_{vy}, C^*_{vx}, C^*_{vy}) of the rotational hydrodynamic forces in phase with the cylinder angular velocities. To capture the fluid force fluctuation nature, both root-mean squared (′) and maximum (*) forces are evaluated, providing a practical data range of potential coefficients. Overall results in Fig. 14 emphasize the effect of cylinder curvature versus flow direction. It can be seen that the maximum coefficients in both in-line (Figs. 14a and 14c) and cross-flow (Figs. 14b and 14d) directions are associated with the perpendicular flows entailing the maximum response amplitudes shown in Figs. 3a and 3b. The minimum coefficients are associated with the convex flows. Both Figs. 3 and 14 exhibit similar diagram features according to the coupled fluid-structure interactions whose magnified excitation coefficients are within the main lock-in ranges. Their maximum $C^*_{vx} \approx 1.5$ and $C^*_{vy} \approx 3.5$ values are comparable to those reported in other 2-DOF VIV experimental [27] and analytical prediction [20] studies.

With varying V_r, Fig. 15 plots the added inertia coefficients (C'_{ax}, C'_{ay}, C^*_{ax}, C^*_{ay}) of the rotational hydrodynamic forces in phase with the cylinder angular accelerations. Essentially, overall results reveal the typical transition of the non-constant added inertia from (i) having a positive value at the beginning of the lock-in ($V_r \approx 4$), (ii) approaching a zero at the resonance frequency associated with the response peak region (around $6<V_r<10$), and (iii) deviating asymptotically, at a higher V_r, to a certain negative value of about -1 for cross-flow VIV (Figs. 15b and 15d) and -0.5 for in-line VIV (Figs. 15a and 15c). Consistently, the cylinder oscillation frequencies increase with the decreasing added inertia when increasing V_r as illustrated in Fig. 11. Such added inertia tendency found in the present pendulum system of the curved cylinder VIV is qualitative similar to what has been experimentally observed for the added mass coefficients of the non-pivoted straight cylinder VIV with one [56, 57] or two [53, 54] DOF.

To further facilitate the comparisons of hydrodynamic properties, the total force components in in-line (C'_x, C^*_x) and cross-flow (C'_y, C^*_y) directions are now evaluated so as to estimate their qualitative trends with varying V_r as presented in Fig. 16 for all cylinder cases. In addition, in-line (C_{xm}) and cross-flow (C_{ym}) mean force coefficients are also plotted in Figs. 16e and 16f, respectively. Note that coefficients C'_x, C'_y and C_{xm} from the 2-DOF straight cylinder VIV tests of Jauvtis and Williamson [24] are also compared in Figs. 16a, 16c and 16e. Results reveal that the maximum force coefficients are associated with cross-flow VIV in the perpendicular flow case, with the greatest $C^*_y \approx 4.3$ (Fig. 16d) and $C^*_x \approx 1.8$ (Fig. 16b). Also, the perpendicular flow has a greater maximum $C'_y \approx 3$ (Fig. 16c) than $C'_y \approx 2$ of the straight cylinder, yielding a greater maximum A_y/D in the former case (Fig. 3d). Both experiments have a similar maximum C'_x (1.3-1.5), hence yielding comparable A_x/D responses (Fig. 3c), as well as a similar upper-branch response range ($4< V_r < 10$) owing to the similarly low value m^* (1.9 and 2.6) and ξ_w (2%-4%). The presented fluctuation force coefficients in the oscillating curved cylinder cases are indeed greater than those (< 1) reported in the stationary curved cylinder cases [10-13].

As for the mean forces accounting for the drag amplification due to VIV, both perpendicular and

straight-cylinder experiments have a comparable maximum $C_{xm} \approx 3$ (Fig. 16e). A maximum $C_{ym} \approx 0.24$ can be recognised in the perpendicular flow case (Fig. 16f). The mean lift (in-plane) force coefficients have also been reported in [10, 11] for stationary cylinders although at much lower Re =100 and 500. Overall, the minimum cross-flow/in-line force coefficients correspond to the convex case, producing the minimum A_x/D (Fig. 3a) and A_y/D (Fig. 3b) responses as well as the minimum static drifts (Figs. 7a and 7c). With Re = 3900, Gallardo et al. [12] have reported that for a stationary convex cylinder $C_{xm} \approx 0.74$ which is comparable to $C_{xm} \approx 0.75$ in Fig. 16e as $V_r > 10$ for the oscillating convex cylinder with a very small A_y/D (Fig. 3b). Based on the above-mentioned results, it is expected that the convex (perpendicular) flow case would represent the least (most) impactful fluid-structure interaction scenario for a deep-water installation of a cylindrical structure undergoing VIV due to current flows.

In Fig. 17, several eight-shaped trajectories plotted through the time-varying C_x-C_y coefficient relationships under multiple 2:1:1 resonances are displayed for the selected V_r = 6.02, 6.74, 7.14 and 8.04 in the perpendicular flow case (Fig. 12). Due to the fluid-structure interactions, a strong modulation in both the response amplitudes and relative phases is observed, affecting the repeatability of the two-dimensional trajectories (see also Fig. 8). By plotting about 10 periods of the primary cross-flow oscillation frequencies, the averaged phase difference θ_{xy} values associated with Figs. 17a to 17d are about 1.01π, 1.18π, 1.23π and 1.30π, with the phase variations of about ±2, ±3, ±5 and ±6%, respectively. These phase envelopes exemplify the variable repeatability level of trajectories as a function of V_r. Overall asymmetric features and variable X-Y phase differences in both cylinder (Fig. 8) and force responses (Fig. 17) suggest the complex fluid wake patterns which call for a further detailed three-dimensional numerical simulation and flow visualization investigation.

5. Conclusions

Two-degree-of-freedom in-plane and out-of-plane VIV responses of a rigid curved circular cylinder with a low mass ratio and damping ratio have been experimentally investigated to understand the fundamental effect of cylinder curvature in relation to the approaching flow direction. Three curved cylinder configurations in parallel concave/convex and perpendicular flows in a subcritical range with a maximum Re of about 50,000 have been considered. With varying flow velocities, experimental results of cross-flow/in-line VIV have been presented in terms of the cylinder response amplitudes, inclination angles, mean displacements, motion trajectories, oscillation frequencies, hydrodynamic forces, relative phases, fluid excitation and added inertia coefficients. Comparisons of experimental data with previous results from VIV tests of curved and straight cylinders have also been presented.

It is found that the cylinder curvature, leading to the system asymmetry, plays an influential role in the combined cross-flow/in-line VIV responses revealing some interesting fluid-structure interaction features. In the perpendicular flow case, the appearance of multiple 2:1:1 resonance involving two in-line (out-of-plane) and one cross-flow (in-plane) predominant oscillation frequencies is meaningful which renders the asymmetric figure-of-eight motion trajectories for both cylinder and hydrodynamic force responses. In all curved cylinder tests, variable local inclination angles inclusive of initial, mean

and oscillation components are also presented. For perpendicular flows, cross-flow mean displacements due to the associated cross-flow mean forces are noticed in addition to the typical in-line counterparts. The perpendicular (convex) flow case exhibits the maximum (minimum) in-plane and out-of-plane VIV whereas the concave flow case reveals the sustained lower-branch responses in a wider velocity range which may be attributed to the wake-induced instability generated from a leading horizontal section.

Experimental hydrodynamic forces and relative phases governing the fluid-structure interactions are evaluated, providing new datasets of the fluid excitation and added inertial coefficients as a function of the reduced velocity and the flow orientation versus the cylinder curvature plane. These hydrodynamic coefficients could be applied to the prediction models and practical design codes for curved cylindrical structures undergoing VIV. Flow visualisation studies should be further carried out to characterise the wake vortex-shedding patterns. More experiments are needed to capture other key aspects including the curvature radius ratio, mass ratio, damping ratio, aspect ratio, Re and oblique flows. Understanding of a curved rigid cylinder VIV can be useful for a more advanced VIV analysis of curved flexible cylinders.

Acknowledgements: The authors would like to thank experimental facilities and technicians at the Kelvin Hydrodynamics Laboratory, and Mr Safrendyo at Newcastle University for a drawing in Fig. 1. Insightful and constructive comments from anonymous reviewers are gratefully acknowledged.

Appendix: Estimation of Hydrodynamic Forces and Coefficients

The hydrodynamic forces and coefficients associated with the pivoted cylinder-spring system shown in Fig. 1 are estimated based on the equilibrium of angular momenta of forces [50]. For a small value of the global vertical (roll or pitch) deflection angle about the pivot (φ), the equation of motion of the pendulum system including vertical, curved and horizontal parts may be written in a generic form as

$$I\ddot{\varphi} = M_b - M_w - M_s - M_d + M_h, \tag{A.1}$$

where a dot denotes differentiation with respect to time. About the pivot, I (I=I_V+I_C+I_H) is the total moment of inertia of the pendulum combining the vertical (I_V), curved (I_C) and horizontal (I_H) parts, $M_b \approx \left(\rho g \pi D^3/4\right)(10\pi/4+3)L_b\varphi$ the moment of the buoyancy force, $M_w = MgL_w\varphi$ the moment of the cylinder gravity force, $M_s = F_sL_s$ the moment of the spring's restoring force, $M_d = cL_s^2\dot{\varphi}$ the moment of the structural damping force, M_h the moment of the total hydrodynamic force, D the cylinder diameter, L_b the moment arm from the pivot to the centre of buoyancy, L_w the moment arm from the pivot to the centre of gravity of the pendulum, M the total pendulum mass, g the gravity acceleration, F_s the resulting spring force measured by the load cells, L_s the moment arm from the pivot to the location of spring attachment and c the structural damping coefficient estimated through a free decay test in air.

For the in-air vertical cylinder with upper and lower parts of different properties, the associated moment of inertia (I_V), valid in both in-plane/out-of-plane oscillation cases, reads [58]

$$I_V = \frac{1}{3}M_UL_U^2 + \frac{1}{12}M_LL_L^2 + M_L\left(L_U + L_L/2\right)^2, \tag{A.2}$$

in which M_U (M_L) is the mass and L_U (L_L) is the length of the upper (lower) part. For the submerged sections, the moment of inertia of the curved (I_C) and horizontal (I_H) parts in the case of *in-plane* oscillation may be approximated by

$$I_C = \left\{\left((5D)^2 + \frac{3}{4}\left(\frac{D}{2}\right)^2\right) + \left(L_U + L_L + 10D/\pi\right)^2 + \left(5D - 10D/\pi\right)^2\right\}\left(M_C + 5D\rho\pi\left(\frac{D}{2}\right)^2\right), \quad \text{A.3}$$

$$I_H = \left\{\frac{1}{12}(3D)^2 + \left(5D + 3D/2\right)^2 + {L_H}^2\right\}\left(M_H + \frac{4}{3}\rho\left(\frac{D}{2}\right)^3\right), \quad \text{A.4}$$

where M_C is the mass of the curved cylinder, M_H the mass of the horizontal extension and L_H the vertical distance from the pivot to the centre line of the horizontal cylinder. In the case of *out-of-plane* oscillation, I_C and I_H may be approximated by

$$I_C = \left\{\frac{1}{8}\left(4(5D)^2 + 5\left(\frac{D}{2}\right)^2\right) + \left(L_U + L_L + 10D/\pi\right)^2\right\}\left(M_C + \frac{\pi D}{4}\rho\pi\left(\frac{D}{2}\right)^2\right), \quad \text{A.5}$$

$$I_H = \left\{\frac{D^2}{8} + {L_H}^2\right\}\left(M_H + 3D\rho\pi\left(\frac{D}{2}\right)^2\right). \quad \text{A.6}$$

In this study, the vertical hydrodynamic force is neglected because of the horizontal planar spring arrangement and the small vertical angles. Only the total horizontal hydrodynamic force (F_h) is considered and its centre is assumed to be fixed at a neutral point of the submerged body. Accordingly, the integral of the fluid force per unit length, multiplied by the moment arm, over the cylinder projected span length entails $M_h \approx F_h L_{hd}$ where, in the in-plane oscillation case,

$$L_{hd} \approx L_U + L_L + 10D/\pi, \quad \text{A.7}$$

whereas, in the out-of-plane oscillation case,

$$L_{hd} \approx L_U + L_L + (10DM_C/\pi + 5DM_H)/(M_C + M_H). \quad \text{A.8}$$

By balancing overall structural and fluid moments, F_h can be obtained through A.1, and the associated coefficient of total hydrodynamic force (C_h) – comprising oscillatory and mean components in either in-plane or out-of-plane direction – may be extracted from

$$C_h = \frac{2F_h}{\rho V^2 D^2 (5\pi/2 + 3)}. \quad \text{A.9}$$

Note that the effect of two-dimensional stiffness cross-coupling is herein neglected as in [50]. This is feasible since Kheirkhah et al. [49] showed that a pendulum 2-DOF VIV exhibiting figure-of-eight, 2:1 resonant trajectories is associated with a weak stiffness coupling.

To assess the phase differences (θ_x, θ_y) between the cylinder rotational response (φ_x, φ_y) and the fluid force moments (M_{hx}, M_{hy}), the phase differences between cross-flow and in-line motions (θ_{xy}), and the hydrodynamic coefficients in phase with the cylinder angular velocities (C_{vx}, C_{vy}) and accelerations (C_{ax}, C_{ay}), cross-flow (φ_y, M_{hy}) and in-line (φ_x, M_{hx}) responses may be approximated to be sinusoidal at a primary resonant oscillation frequency ω. Hence, the steady-state responses of A.1 may be postulated through a harmonic function as

$$\varphi_y = \varphi_{0y}\sin(\omega_y t), \qquad M_{hy} = M_{hy0}\sin(\omega_y t + \theta_y), \quad \text{A.10}$$

$$\varphi_x = \varphi_{0x}\sin(\omega_x t + \theta_{xy}), \qquad M_{hx} = M_{hx0}\sin(\omega_x t + [\theta_x + \theta_{xy}]), \tag{A.11}$$

with the rotational response (φ_{0y}, φ_{0x}) and moment (M_{hy0}, M_{hx0}) amplitudes. The moment in A.10 or A.11 can also be decomposed into a component in phase with the cylinder angular velocity and acceleration, and rewritten in a generic form, by omitting the subscript *x* or *y* for brevity, as

$$M_h = M_{h0}\sin\theta\cos\omega t + M_{h0}\cos\theta\sin\omega t, \tag{A.12}$$

By substituting A.10 (or A.11) and A.12 into A.1 and applying the harmonic balance, the phase difference (θ) can be expressed in a generic form, valid for both *x* or *y* motion, as

$$\theta = \tan^{-1}\left[\frac{cL_s^2\omega}{\left\{\left(M_w + M_s - M_b\right)/\varphi_0 - \omega^2 I\right\}}\right]. \tag{A.13}$$

By combining the second right-hand term in A.12 with the left-hand term in A.1, and by considering the added moment of inertia equal to C_aI [50] where I accounts for the submerged parts (i.e., $I_C + I_H$), the added inertia coefficient C_a may be approximated as

$$C_a \approx \left[\frac{M_{h0}\cos\theta}{\left(I_C + I_H\right)\omega^2\varphi_0}\right]. \tag{A.14}$$

By considering the excitation force being proportional to the dynamic pressure [59] and, hence, approximately equating the first right-hand term in A.12 to the total force moment ($\rho C_V DV^2 L_{sub}/2$)L_{hd} where L_{sub} is the total submerged length and L_{hd} is the moment lever (A.7 or A.8), the coefficient of the force moment in phase with the cylinder angular velocity may be approximated as

$$C_v \approx \left[\frac{M_{h0}\sin\theta}{\rho DV^2 L_{sub}L_{hd}/2}\right]. \tag{A.15}$$

Depending on the cylinder orientation, associated physical properties and experimental responses, expressions A.13-A15 can be applied to both cross-flow and in-line directions. It is worth noting that, without knowing the actual time-varying centres of fluid forces acting on the submerged oscillating cylinder, the present simplified formulation enables the analysis of qualitative trends of hydrodynamic properties by comparing different flow-curvature configuration cases as in Section 4 in relation to the measured response amplitudes and frequencies presented and discussed in Section 3.

References

[1] T. Sarpkaya, A critical review of the intrinsic nature of vortex-induced vibrations, Journal of Fluids and Structures, 19 (2004) 389-447.

[2] P.W. Bearman, Circular cylinder wakes and vortex-induced vibrations, Journal of Fluids and Structures, 27 (2012) 648-658.

[3] X. Wu, F. Ge, Y. Hong, A review of recent studies on vortex-induced vibrations of long slender cylinders, Journal of Fluids and Structures, 28 (2012) 292-308.

[4] C.H.K. Williamson, R. Govardhan, Vortex-induced vibrations, Annual Review of Fluid Mechanics, 36 (2004) 413-455.

[5] R.D. Gabbai, H. Benaroya, An overview of modeling and experiments of vortex-induced vibration of circular cylinders, Journal of Sound and Vibration, 282 (2005) 575-616.

[6] N. Srinil, Multi-mode interactions in vortex-induced vibrations of flexible curved/straight structures with geometric nonlinearities, Journal of Fluids and Structures, 26 (2010) 1098-1122.
[7] N. Srinil, M. Wiercigroch, P. O'Brien, Reduced-order modelling of vortex-induced vibration of catenary riser, Ocean Engineering, 36 (2009) 1404-1414.
[8] H. Zanganeh, N. Srinil, Three-dimensional VIV prediction model for a long flexible cylinder with axial dynamics and mean drag magnifications, Journal of Fluids and Structures, 66 (2016) 127-146.
[9] W.J. Kim, N.C. Perkins, Two-dimensional vortex-induced vibration of cable suspensions, Journal of Fluids and Structures, 16 (2002) 229-245.
[10] A. Miliou, S.J. Sherwin, J.M.R. Graham, Fluid dynamic loading on curved riser pipes, Journal of Offshore Mechanics and Arctic Engineering, 125 (2003) 176-182.
[11] A. Miliou, A. De Vecchi, S.J. Sherwin, J.M.R. Graham, Wake dynamics of external flow past a curved circular cylinder with the free stream aligned with the plane of curvature, Journal of Fluid Mechanics, 592 (2007) 89-115.
[12] J.P. Gallardo, H.I. Andersson, B. Pettersen, Turbulent wake behind a curved circular cylinder, Journal of Fluid Mechanics, 742 (2014) 192-229.
[13] T. Xu, J.E. Cater, Numerical simulation of flow past a curved cylinder in uniform and logarithmic flow, Ships and Offshore Structures, 12 (2017) 323-329.
[14] A. de Vecchi, S.J. Sherwin, J.M.R. Graham, Wake dynamics of external flow past a curved circular cylinder with the free-stream aligned to the plane of curvature, Journal of Fluids and Structures, 24 (2008) 1262-1270.
[15] A. de Vecchi, S.J. Sherwin, J.M.R. Graham, Wake dynamics past a curved body of circular cross-section under forced cross-flow vibration, Journal of Fluids and Structures, 25 (2009) 721-730.
[16] G.R.S. Assi, N. Srinil, C.M. Freire, I. Korkischko, Experimental investigation of the flow-induced vibration of a curved cylinder in convex and concave configurations, Journal of Fluids and Structures, 44 (2014) 52-66.
[17] B. Seyed-Aghazadeh, C. Budz, Y. Modarres-Sadeghi, The influence of higher harmonic flow forces on the response of a curved circular cylinder undergoing vortex-induced vibration, Journal of Sound and Vibration, 353 (2015) 395-406.
[18] N. Srinil, Analysis and prediction of vortex-induced vibrations of variable-tension vertical risers in linearly sheared currents, Applied Ocean Research, 33 (2011) 41-53.
[19] N. Srinil, H. Zanganeh, Modelling of coupled cross-flow/in-line vortex-induced vibrations using double Duffing and van der Pol oscillators, Ocean Engineering, 53 (2012) 83-97.
[20] H. Zanganeh, N. Srinil, Characterization of variable hydrodynamic coefficients and maximum responses in two-dimensional vortex-induced vibrations with dual resonances, Journal of Vibration and Acoustics, 136 (2014) 051010.
[21] N. Srinil, H. Zanganeh, A. Day, Two-degree-of-freedom VIV of circular cylinder with variable natural frequency ratio: Experimental and numerical investigations, Ocean Engineering, 73 (2013) 179-194.

[22] J.M. Dahl, F.S. Hover, M.S. Triantafyllou, Two-degree-of-freedom vortex-induced vibrations using a force assisted apparatus, Journal of Fluids and Structures, 22 (2006) 807-818.
[23] S.-W. Kim, S.-J. Lee, C.-Y. Park, D. Kang, An experimental study of a circular cylinder's two-degree-of-freedom motion induced by vortex, International Journal of Naval Architecture and Ocean Engineering, 8 (2016) 330-343.
[24] N. Jauvtis, C.H.K. Williamson, The effect of two degrees of freedom on vortex-induced vibration at low mass and damping, Journal of Fluid Mechanics, 509 (2004) 23-62.
[25] A. Sanchis, G. Sælevik, J. Grue, Two-degree-of-freedom vortex-induced vibrations of a spring-mounted rigid cylinder with low mass ratio, Journal of Fluids and Structures, 24 (2008) 907-919.
[26] B. Stappenbelt, F. Lalji, G. Tan, Low mass ratio vortex-induced motion, in: The 16th Australasian Fluid Mechanics Conference, Gold Coast, Australia,, 2007, pp. 1491-1497.
[27] G.R. Franzini, R.T. Gonçalves, J.R. Meneghini, A.L.C. Fujarra, One and two degrees-of-freedom Vortex-Induced Vibration experiments with yawed cylinders, Journal of Fluids and Structures, 42 (2013) 401-420.
[28] Y. Bai, Q. Bai, Subsea Engineering Handbook, Elsevier, Oxford, 2012.
[29] W. Ruan, Y. Bai, P. Cheng, Static analysis of deepwater lazy-wave umbilical on elastic seabed, Ocean Engineering, 91 (2014) 73-83.
[30] N. Srinil, Cabling to connect offshore wind turbines to onshore facilities, in: Offshore Wind Farms: Technologies, Design and Operation, Elsevier, 2016, pp. 419-440.
[31] B. Guo, S. Song, A. Ghalambor, T.R. Lin, Offshore Pipelines: Desgin, Installation, and Maintenance, Elsevier, Oxford, 2014.
[32] Handbook on Design and Operation of Flexible Risers, MARINTEK, NTNU, 4Subsea, 2014.
[33] Y. Bai, Q. Bai, Subsea Pipelines and Risers, Elsevier, Oxford, 2005.
[34] R.T. Gonçalves, G.R. Franzini, G.F. Rosetti, J.R. Meneghini, A.L.C. Fujarra, Flow around circular cylinders with very low aspect ratio, Journal of Fluids and Structures, 54 (2015) 122-141.
[35] C.C. Feng, The measurement of vortexinduced effects in flow past stationary and oscillating circular and d-section cylinders, in: MSc Thesis, University of British Columbia, Canada, 1968.
[36] R.E.D. Bishop, A.Y. Hassan, The lift and drag forces on a circular cylinder oscillating in a flowing fluid, in: Proceedings of the Royal Society of London, 1964, pp. 51-75.
[37] A. Khalak, C. Williamson, Motions, forces and mode transitions in vortex-induced vibrations at low mass-damping, Journal of fluids and Structures, 13 (1999) 813-851.
[38] J.T. Klamo, A. Leonard, A. Roshko, The effects of damping on the amplitude and frequency response of a freely vibrating cylinder in cross-flow, Journal of Fluids and Structures, 22 (2006) 845-856.
[39] T.L. Morse, R.N. Govardhan, C.H.K. Williamson, The effect of end conditions on the vortex-induced vibration of cylinders, Journal of Fluids and Structures, 24 (2008) 1227-1239.
[40] K.Y. Kiu, B. Stappenbelt, K.P. Thiagarajan, Effects of uniform surface roughness on vortex-induced vibration of towed vertical cylinders, Journal of Sound and Vibration, 330 (2011) 4753-4763.

[41] B.M. Sumer, J. Fredsoe, Hydrodynamics around cylindrical structures, World Scientific, 2006.
[42] R.D. Blevins, Flow-Induced Vibrations, Van Nostrand Reinhold, New York, 1990.
[43] W.R. Sears, The boundary layer of yawed cylinders, Journal of the Aeronautical Sciences, 15 (1948) 49-52.
[44] S.E. Ramberg, The effects of yaw and finite length upon the vortex wakes of stationary and vibrating circular cylinders, Journal of Fluid Mechanics, 128 (1983) 81-107.
[45] A.R. Hanson, Vortex shedding from yawed cylinders, AIAA Journal, 4 (1966) 738-740.
[46] C.C.W. van Atta, Experiments on vortex shedding from yawed circular cylinders, AIAA Journal, 6 (1968) 931-933.
[47] S.R. Snarski, Flow over yawed circular cylinders: Wall pressure spectra and flow regimes, Physics of Fluids, 16 (2003) 344-359.
[48] M. Zhao, L. Cheng, T. Zhou, Direct numerical simulation of three-dimensional flow past a yawed circular cylinder of infinite length, Journal of Fluids and Structures, 25 (2009) 831-847.
[49] S. Kheirkhah, S. Yarusevych, S. Narasimhan, Orbiting response in vortex-induced vibrations of a two-degree-of-freedom pivoted circular cylinder, Journal of Fluids and Structures, 28 (2012) 343-358.
[50] F. Flemming, C.H.K. Williamson, Vortex-induced vibrations of a pivoted cylinder, Journal of Fluid Mechanics, 522 (2005) 215-252.
[51] C.M. Leong, T. Wei, Two-degree-of-freedom vortex-induced vibration of a pivoted cylinder below critical mass ratio, Proceedings of the Royal Society A: Mathematical, Physical and Engineering Science, 464 (2008) 2907-2927.
[52] G. Schewe, On the force fluctuations acting on a circular cylinder in crossflow from subcritical up to transcritical Reynolds numbers, Journal of Fluid Mechanics, 133 (1983) 265-285.
[53] J.M. Dahl, F.S. Hover, M.S. Triantafyllou, O.H. Oakley, Dual resonance in vortex-induced vibrations at subcritical and supercritical Reynolds numbers, in: Journal of Fluid Mechanics, 2010, pp. 395-424.
[54] J.M. Dahl, Vortex-induced vibration of a circular cylinder with combined in-line and cross-flow motion, in: Department of Mechanical Engineering, MIT, 2008.
[55] Z. Kang, L. Jia, An experiment study of a cylinder's two degree of freedom VIV trajectories, Ocean Engineering, 70 (2013) 129-140.
[56] K. Vikestad, J.K. Vandiver, C.M. Larsen, Added mass and oscillation frequency for a circular cylinder subjected to vortex-induced vibrations and external disturbance, Journal of Fluids and Structures, 14 (2000) 1071-1088.
[57] L.D. Cunha, C.P. Pesce, J. Wanderley, A.L.C. Fujarra, The robustness of the added Mass in VIV models, in: The 25th International Conference on Offshore Mechanics & Arctic Engineering, 2006, pp. 731-738.
[58] S.G. Kelly, Mechanical Vibrations, McGraw-Hill Education, 1996.
[59] L. Kaiktsis, G.S. Triantafyllou, M. Özbas, Excitation, inertia, and drag forces on a cylinder vibrating transversely to a steady flow, Journal of Fluids and Structures, 23 (2007) 1-21.

Table 1 Comparison of numerical and experimental studies on rigid curved circular cylinders

Studies	*R/D*	Cylinders	Re	Cylinder extension part		Motion status
				Horizontal	Vertical	
Miliou et al. (2003)	12.5	PP	100	0	0	Stationary
Miliou et al. (2007)	12.5	CC/CV	100, 500	10*D* (CV)	0, 6*D* (CC)	Stationary
Gallardo et al. (2014)	12.5	CV	3900	10*D*	6*D*	Stationary
Xu & Cater (2017)	12.5	CC/CV	$1x10^5$	0	20*D*	Stationary
de Vecchi et al. (2008)	12.5	CC/CV	100	10*D* (CV)	0	Forced
de Vecchi et al. (2009)	12.5	CV	100	10*D*	0	Forced
Assi et al. (2014)	10	CC/CV	$750\text{-}1.5x10^4$	10*D*	0, 5*D*, 10*D*	Free (2-DOF)
Seyed-Aghazadeh et al. (2015)	47	CC/CV	$300\text{-}2.3x10^3$	0	0	Free (1-DOF)
This study	5	PP/CC/CV	$7x10^3\text{-}5x10^4$	3*D*	0.45*D*	Free (2-DOF)

PP, CC and CV denote perpendicular, concave and convex cylinder configurations, respectively.

Table 2 Comparison of curved cylinder properties for experimental 2-DOF VIV tests

Studies	*m**	ξ_a, ξ_w (%)		f_a, f_w (Hz)	
		In-plane	Out-of-plane	In-plane	Out-of-plane
This study	1.9	0.16^a 2.14^w	0.31^a 2.35^w	0.40^a 0.29^w	0.38^a 0.25^w
Assi et al. (2014)	2.1	0.20^a	0.20^a	-	-

Table 3 Comparison of pivoted cylinder properties from different experimental tests

Studies	*m**	*I**	ξ_{wy} (%)	Re
This study	1.9	24.88	2.14	7300-50000
Flemming and Williamson (2005)	same as *I**	1.03, 2.68, 7.69	3.00	340-2600
Leong and Wei (2008)	0.45	1.41	1.41	820-6050
Kheirkhah et al. (2012)	15.9	66.80	1.10	2100

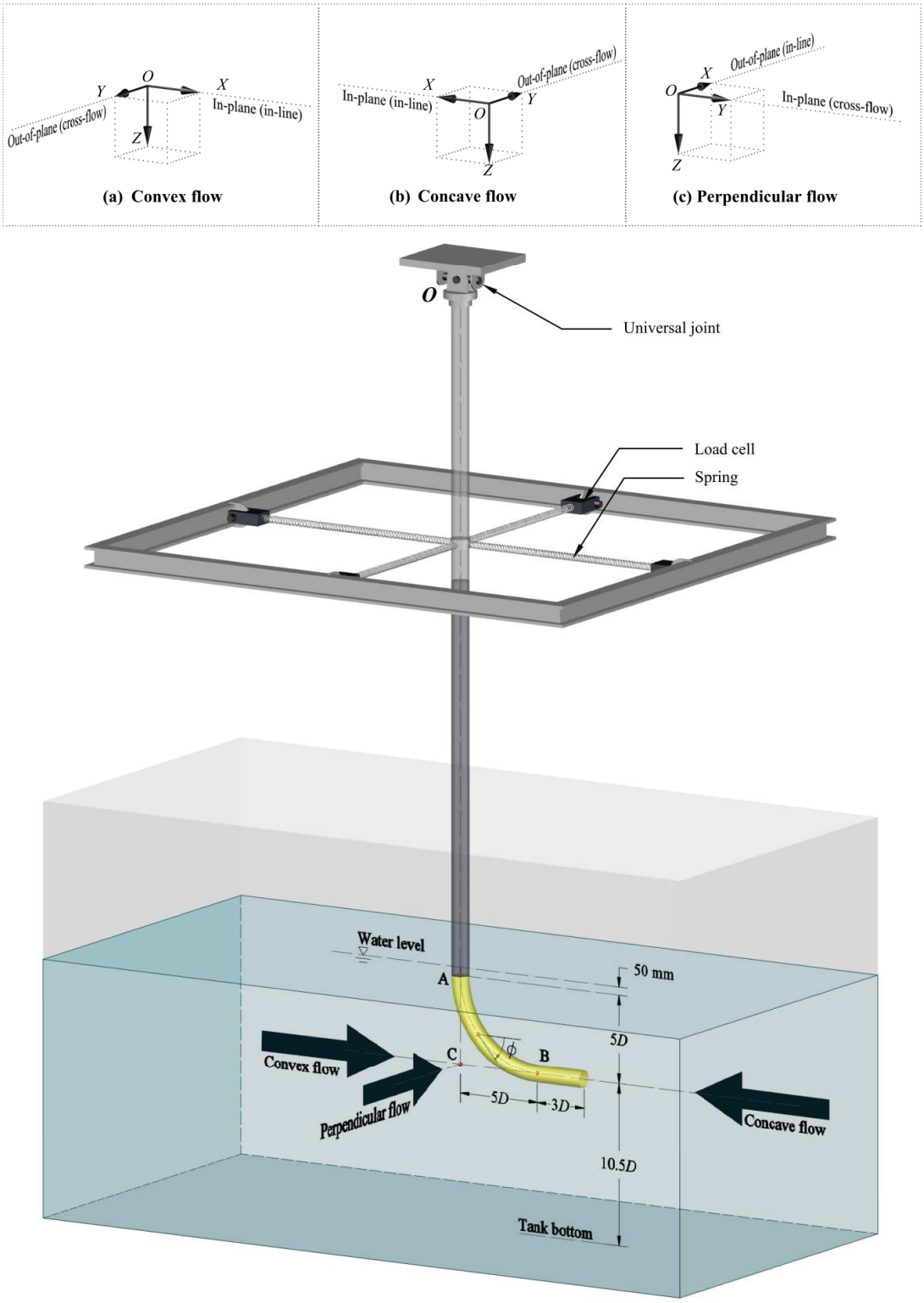

Figure 1 Experiment model and coordinate systems for cross-flow and in-line VIV of a rigid curved cylinder in different parallel (concave/convex) and perpendicular flow orientations.

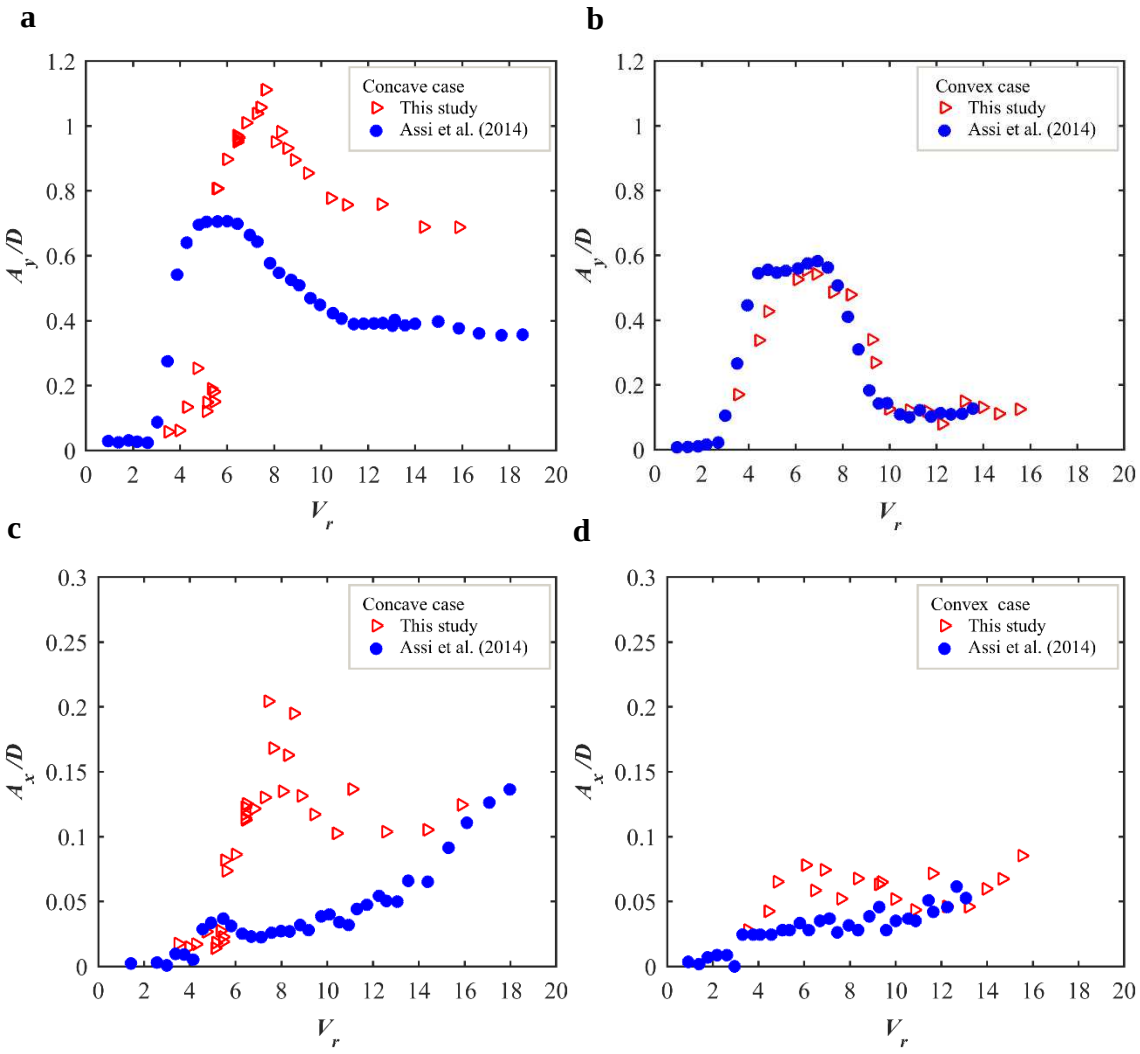

Figure 2 Comparison of experimental results of A_y/D and A_x/D in concave and convex flow cases.

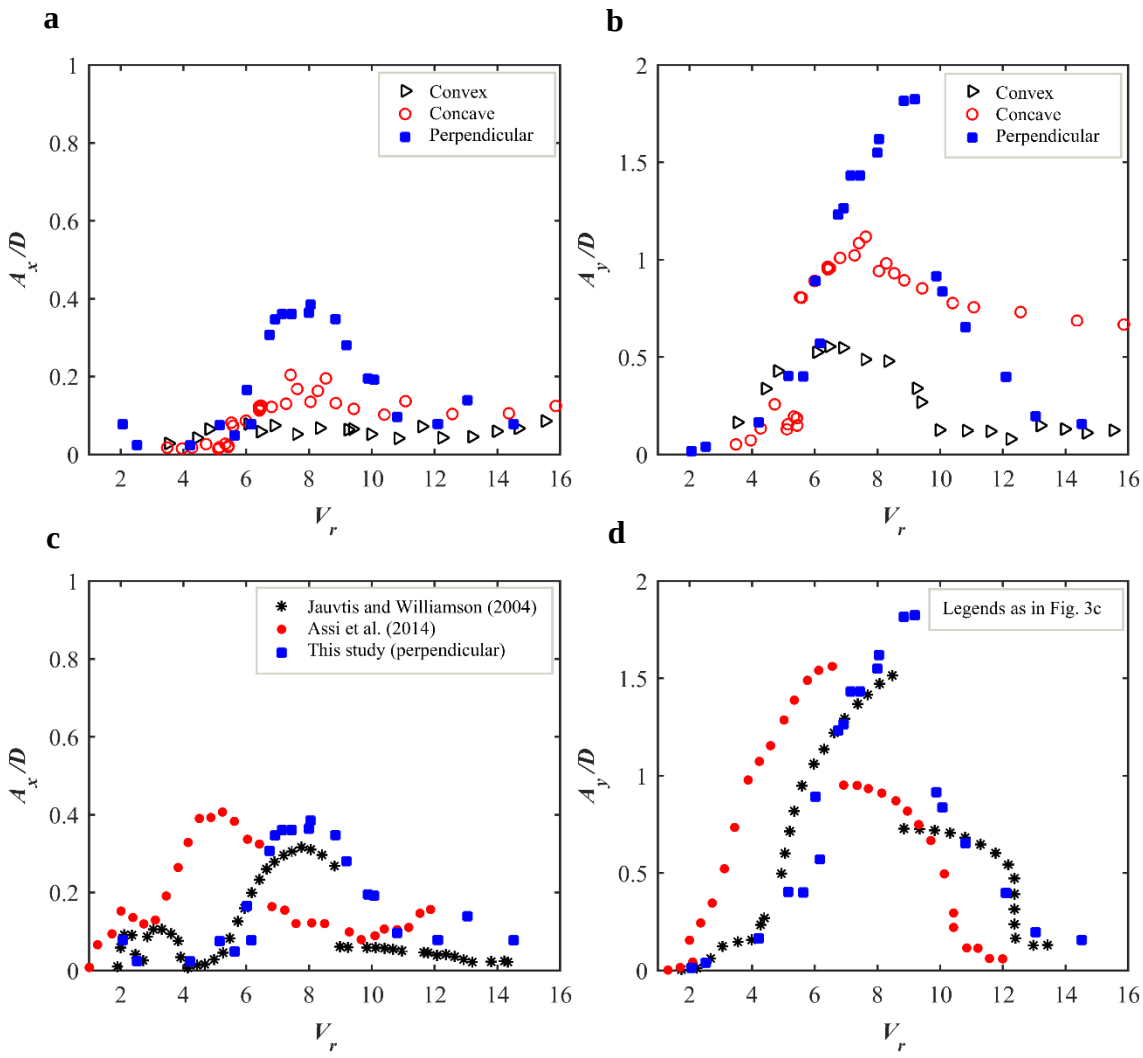

Figure 3 Comparison of experimental results of A_x/D and A_y/D based on (a, b) different flow orientation cases of the present curved cylinder and (c, d) with results of straight cylinder VIV tests.

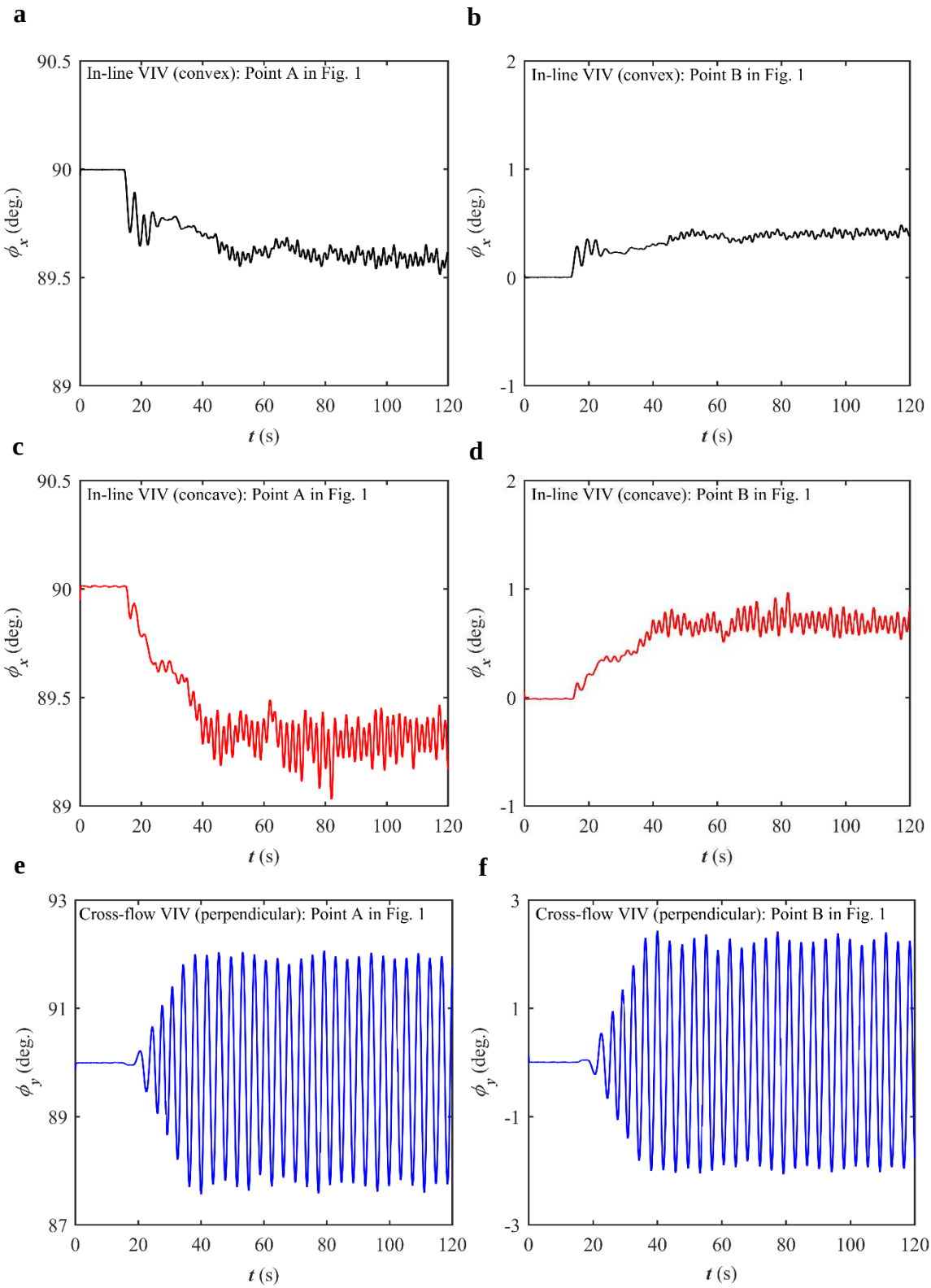

Figure 4 Time-varying local inclination angles inclusive of mean and oscillation components at reference points A and B in Fig. 1 for maximum in-line and cross-flow VIV responses in convex, concave and perpendicular flow cases.

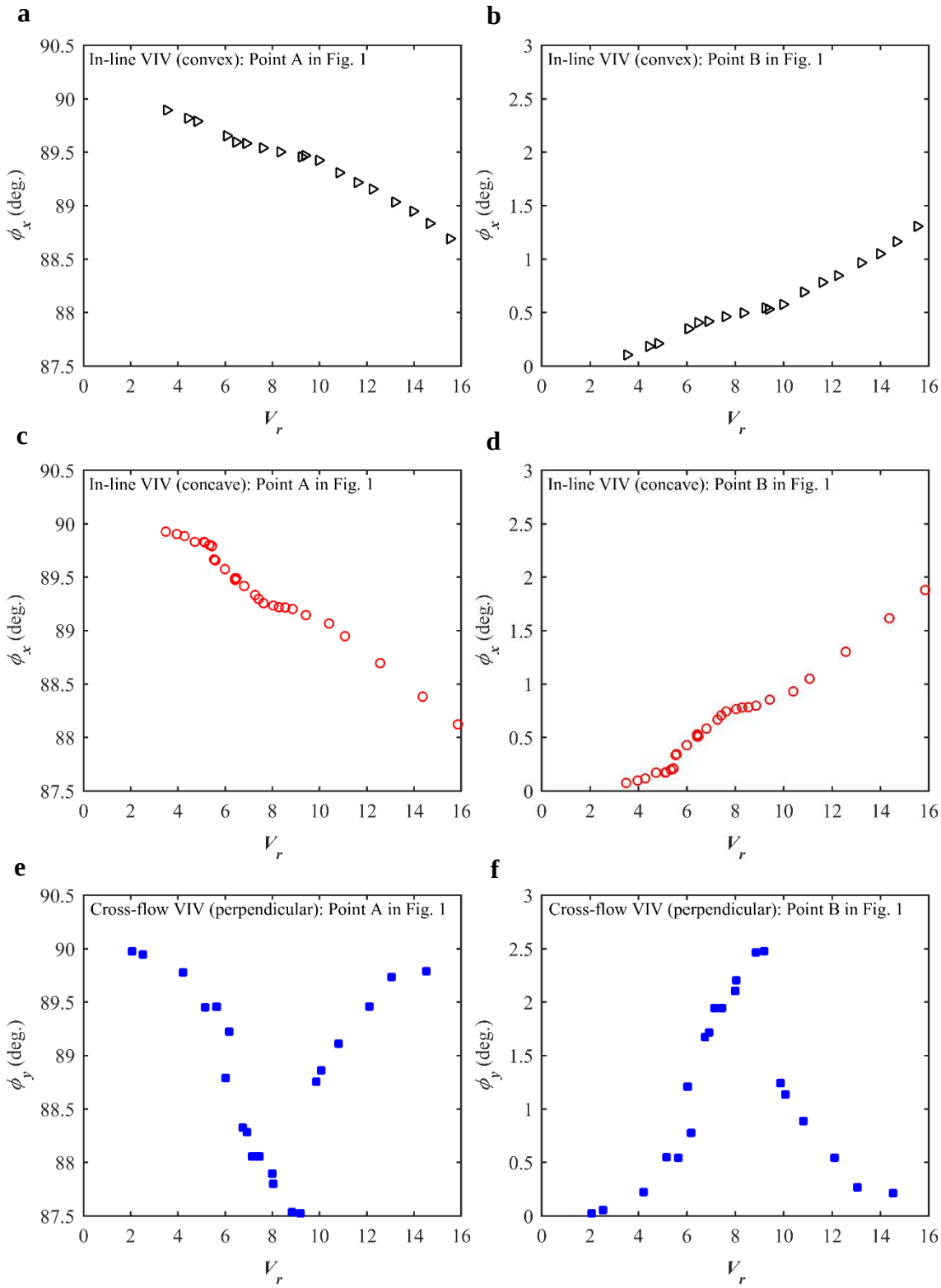

Figure 5 Maximum local inclination angles inclusive of mean and oscillation components at reference points A and B in Fig. 1 for in-line and cross-flow VIV in convex, concave and perpendicular flows.

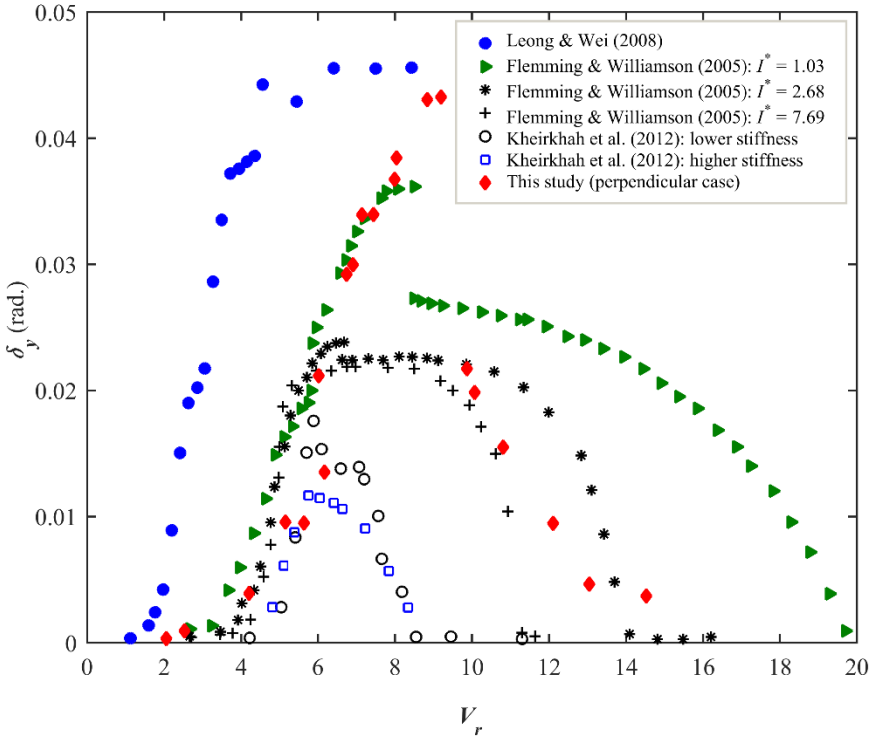

Figure 6 Comparison of maximum global inclination angles of cross-flow oscillations based on different experimental tests of pivoted cylinders.

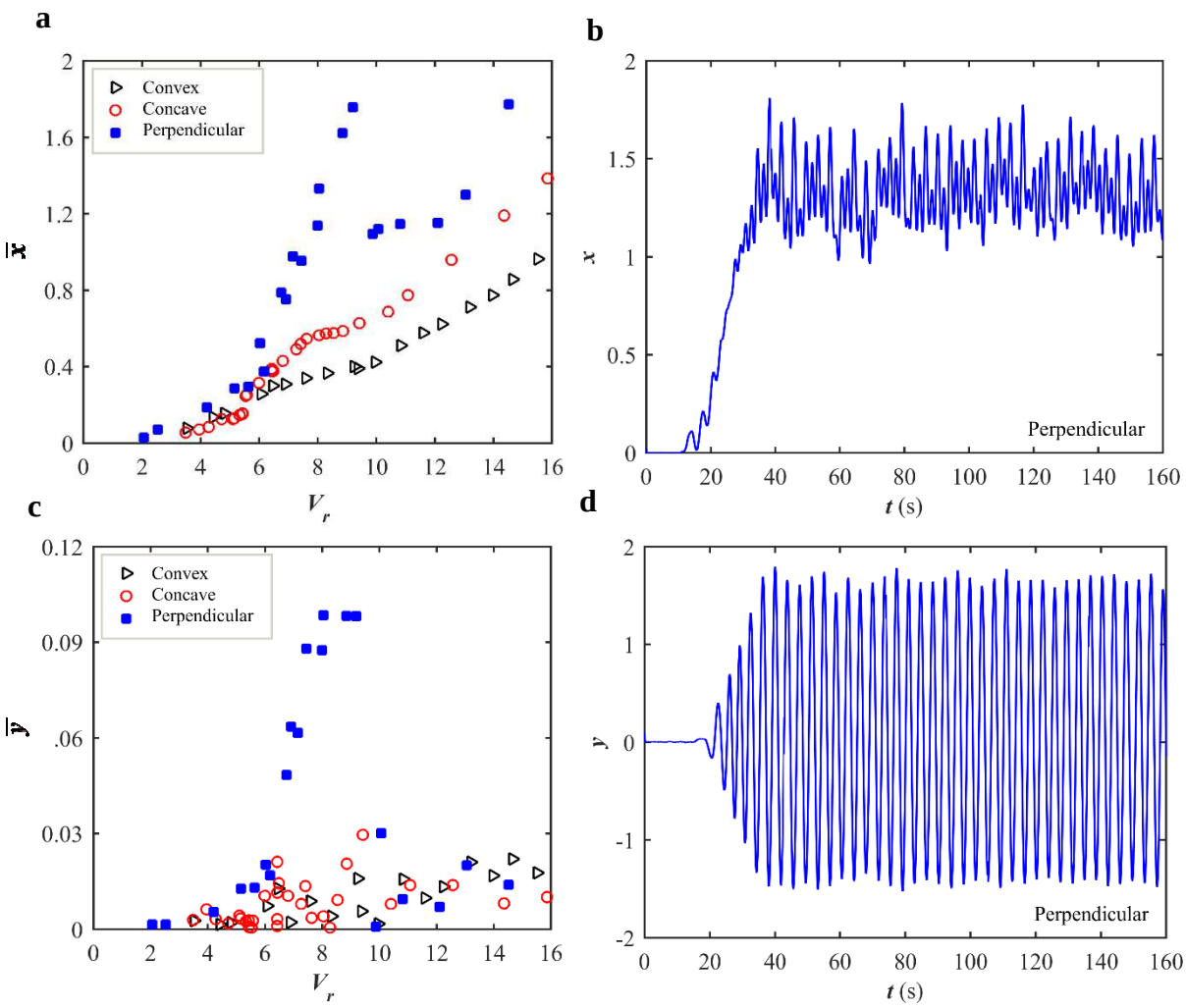

Figure 7 Comparison of (a) in-line and (c) cross-flow mean displacements in different flow orientation cases and with sample response time histories in perpendicular flow case at V_r= 8.04.

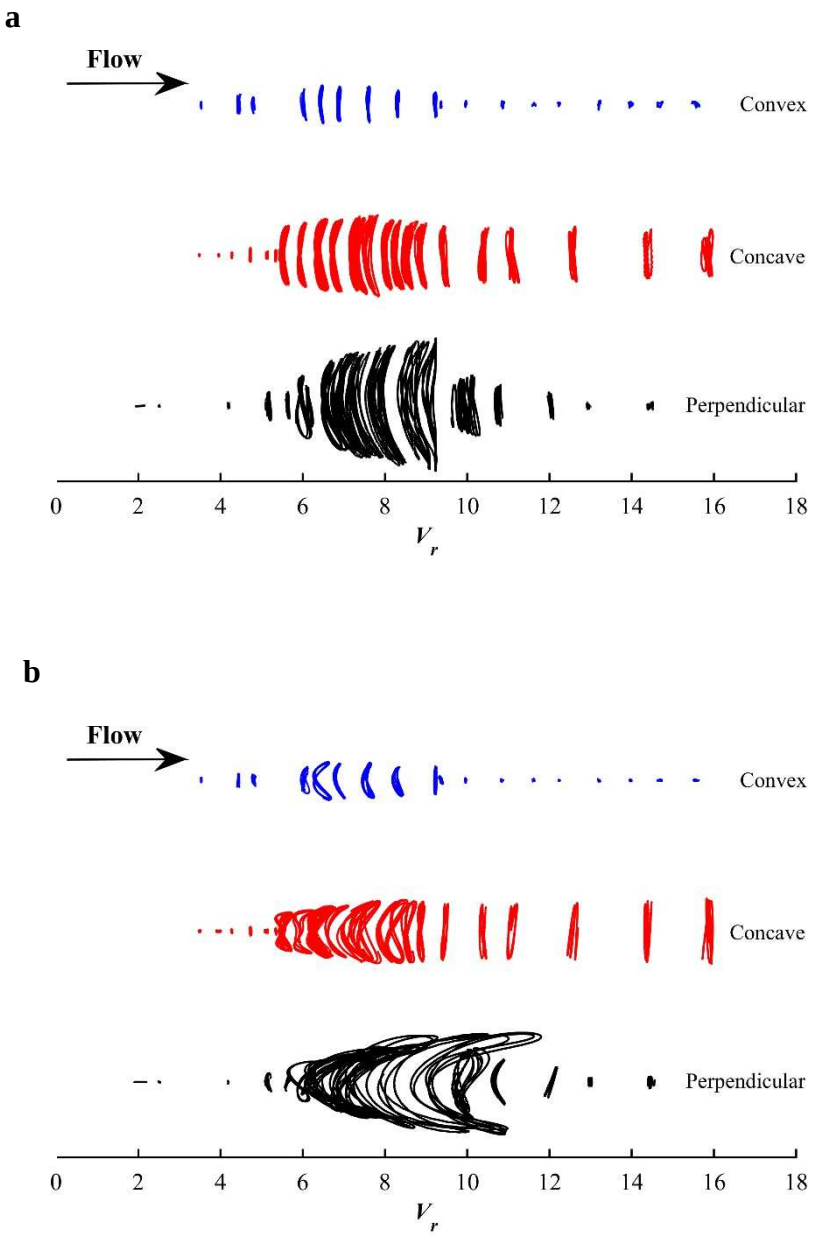

Figure 8 Two-dimensional trajectories of (a) cylinder *X*-*Y* motion and (b) associated hydrodynamic forces in different flow orientation cases.

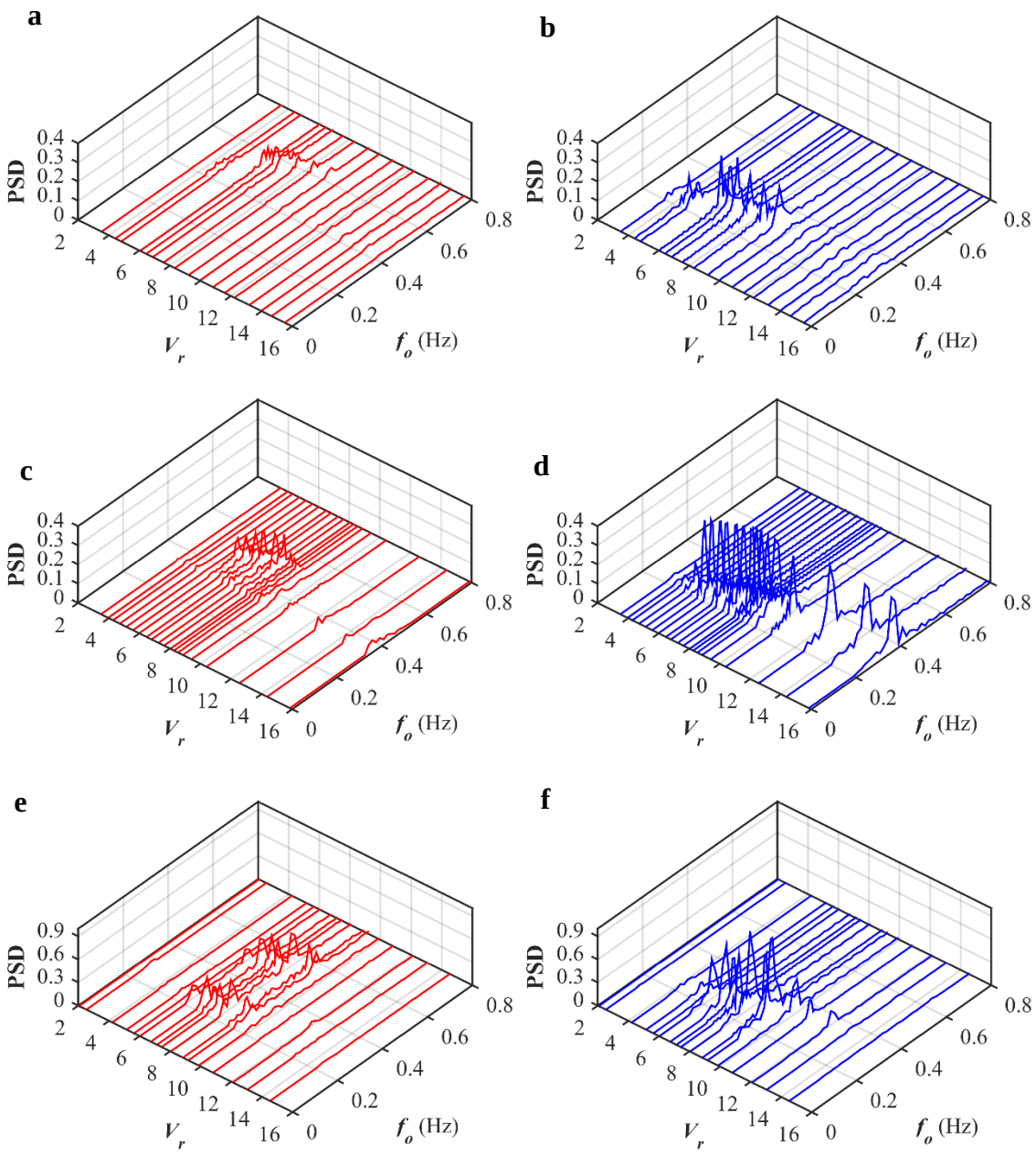

Figure 9 Frequency spectra of (a, c, e) in-line and (b, d, f) cross-flow cylinder responses in convex (a, b), concave (c, d) and perpendicular (e, f) flow cases.

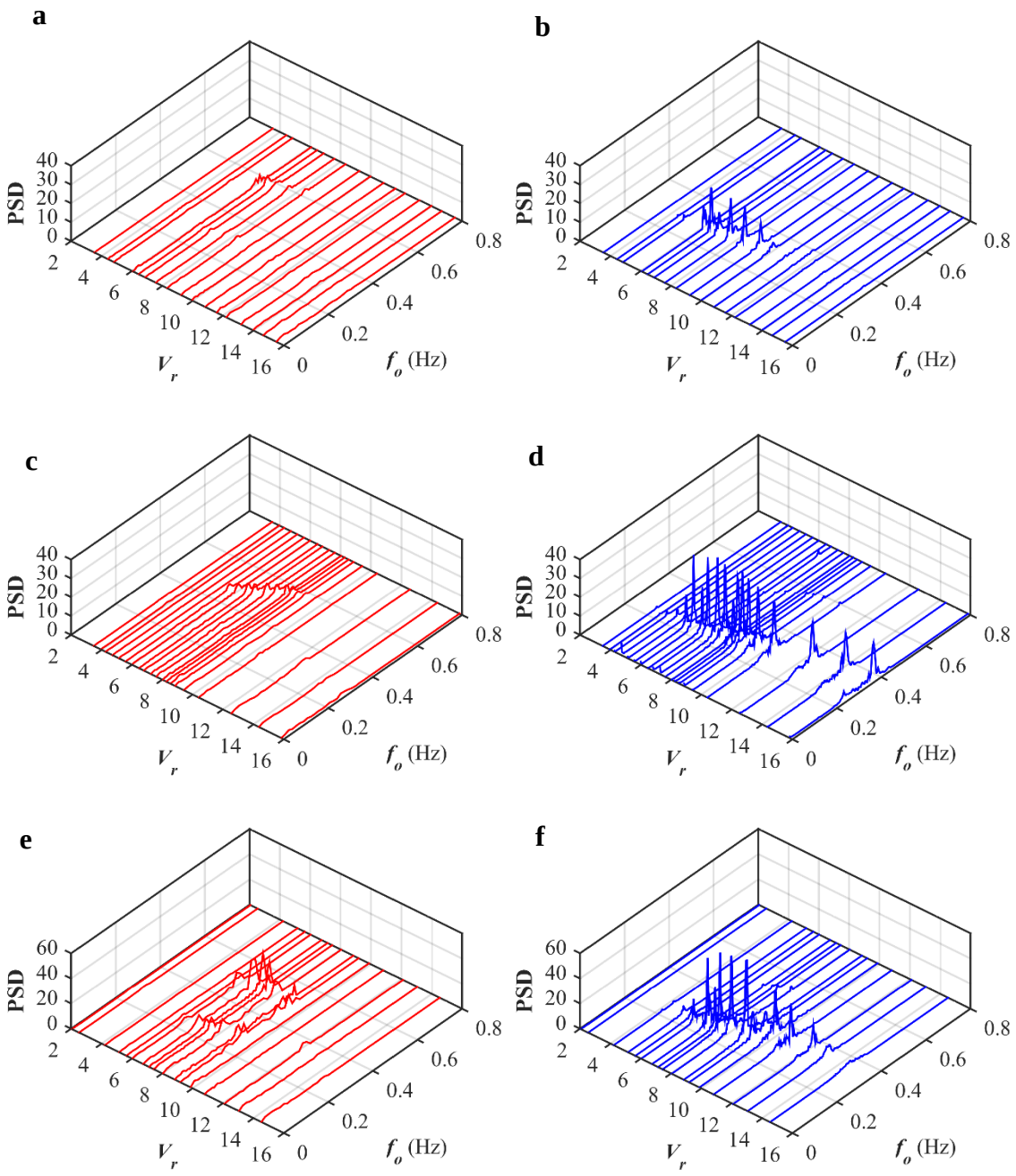

Figure 10 Frequency spectra of (a, c, e) in-line and (b, d, f) cross-flow hydrodynamic forces associated with cylinder responses in Fig. 9 in convex (a, b), concave (c, d) and perpendicular (e, f) flow cases.

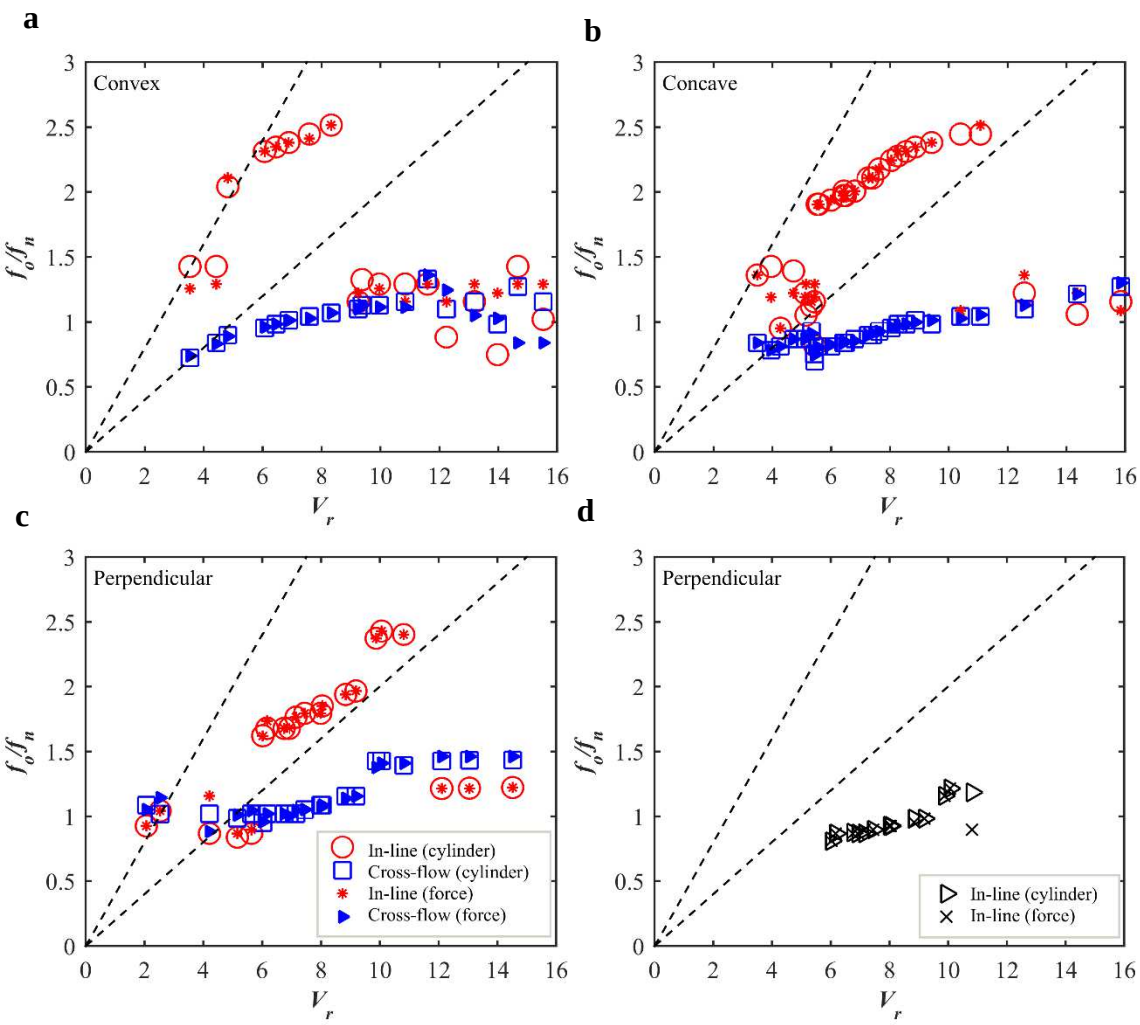

Figure 11 Comparison of in-line and cross-flow oscillation frequency ratios (f_o/f_n) in different flow orientation cases (a-c): a dashed line with slope of 0.2 and 0.4 represents a referenced Strouhal number. For perpendicular flow, f_o/f_n components of secondary in-line frequencies are also plotted in (d).

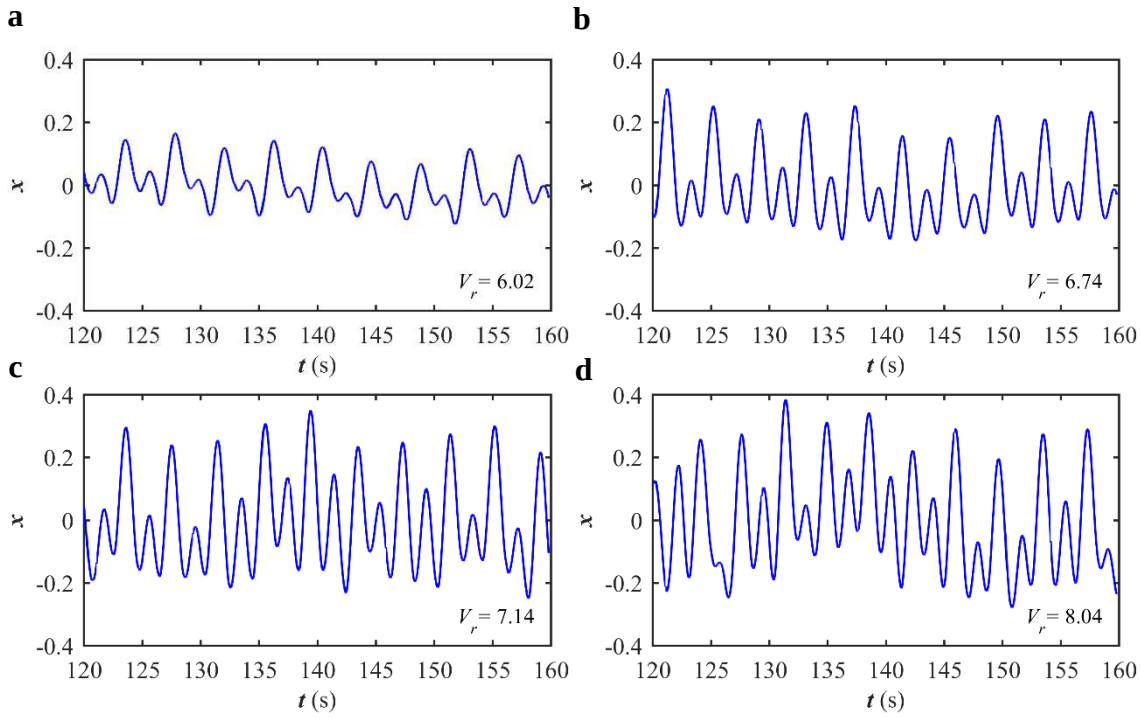

Figure 12 Sample in-line response time histories showing doubled frequencies in perpendicular flow case: (a) V_r = 6.02, (b) V_r = 6.74, (c) V_r = 7.14 and (d) V_r = 8.04.

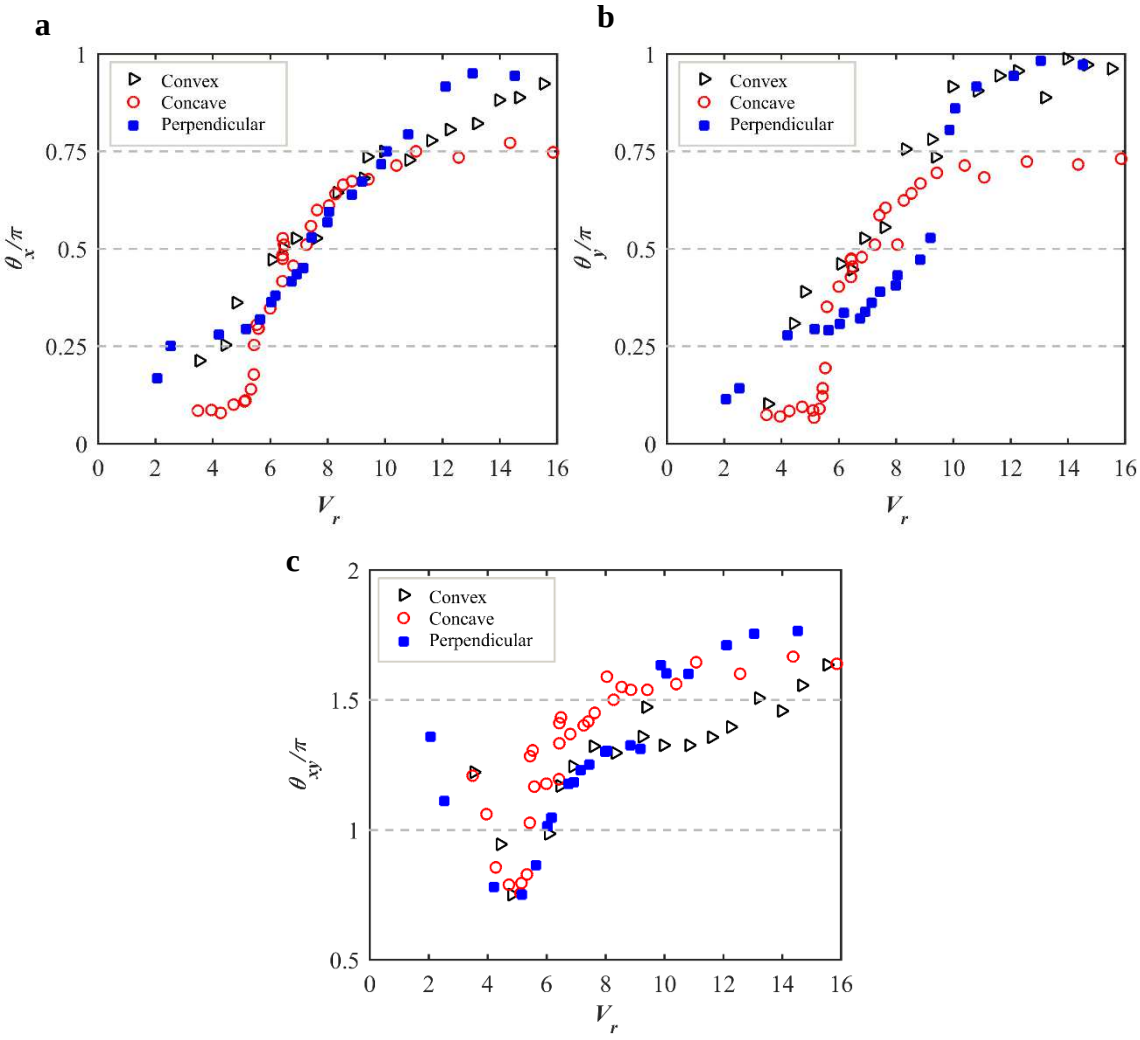

Figure 13 Phase differences between hydrodynamic forces and cylinder responses in (a) in-line and (b) cross-flow directions, and associated *x*-*y* phase differences in different flow orientations.

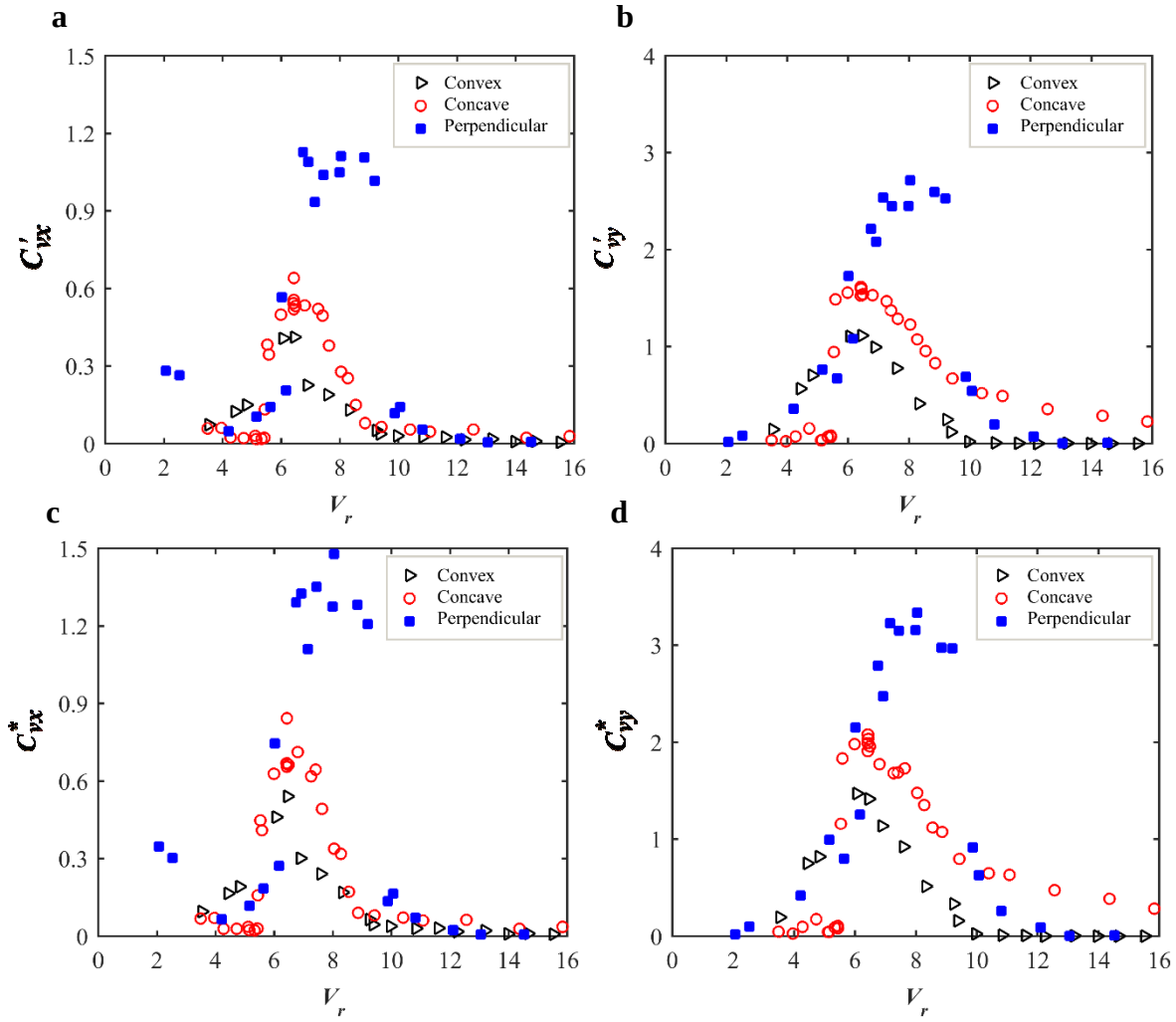

Figure 14 In-line and cross-flow fluid excitation coefficients based on (a, b) root-mean squared and (c, d) maximum values of hydrodynamic forces in phase with cylinder angular velocities in different flow orientations.

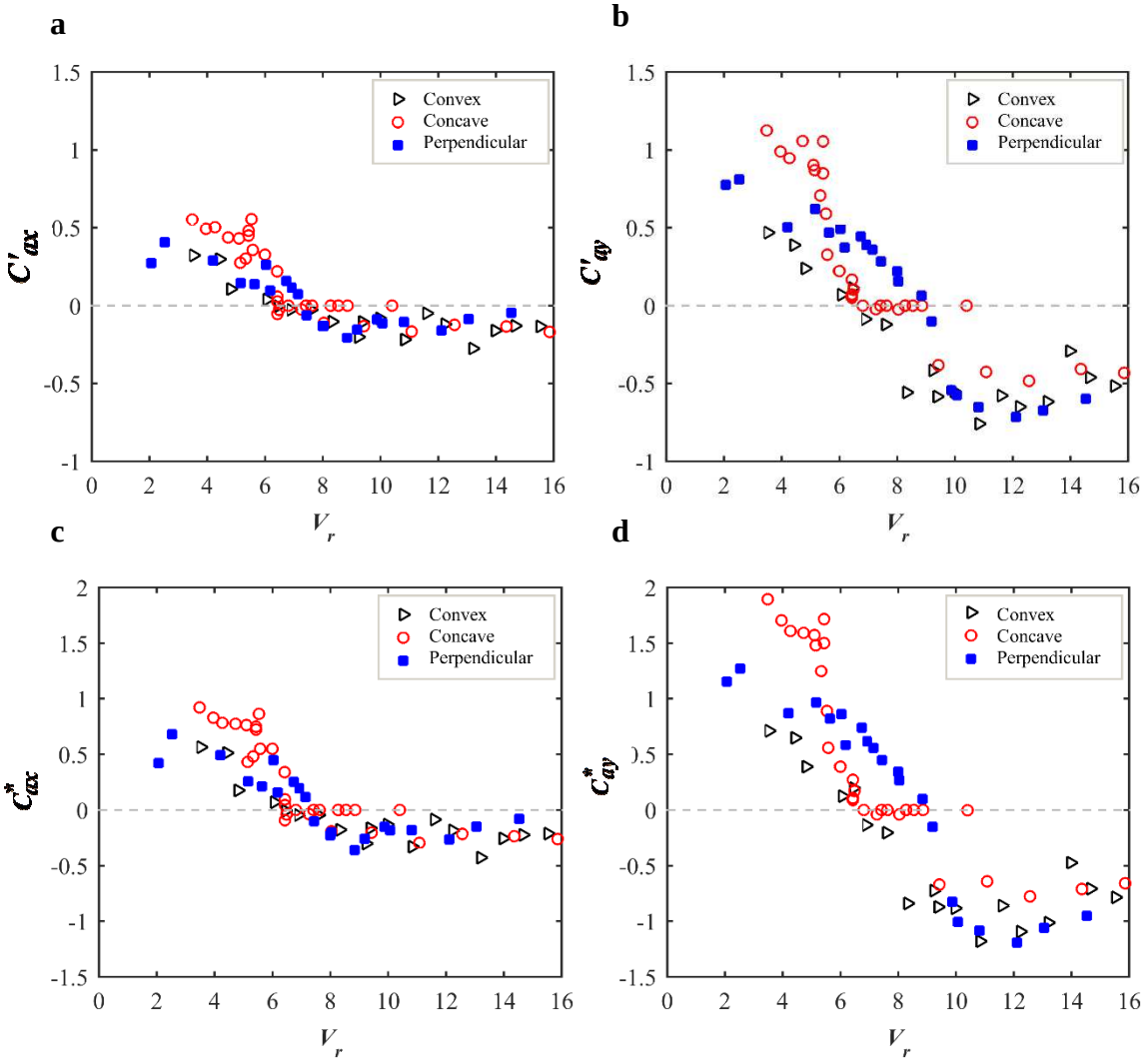

Figure 15 In-line and cross-flow added moment of inertia coefficients based on (a, b) root-mean squared and (c, d) maximum values of hydrodynamic forces in phase with cylinder angular accelerations in different flow orientations.

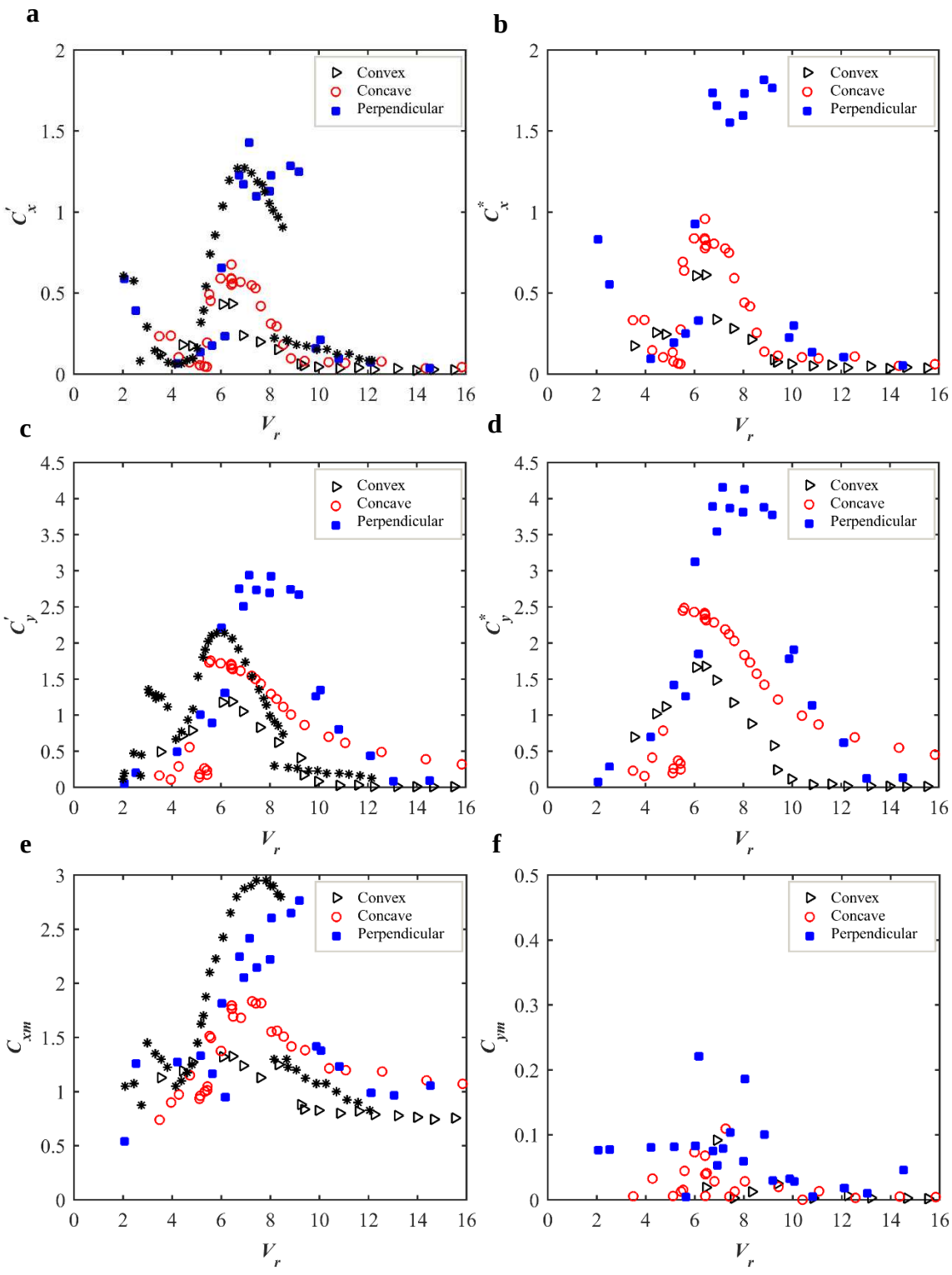

Figure 16 In-line and cross-flow hydrodynamic coefficients based on (a, c) root-mean squared, (b, d) maximum and (e, f) mean values of total fluid forces: stars in (a, c, e) denote results from straight cylinder tests (Jauvtis and Williamson, 2004).

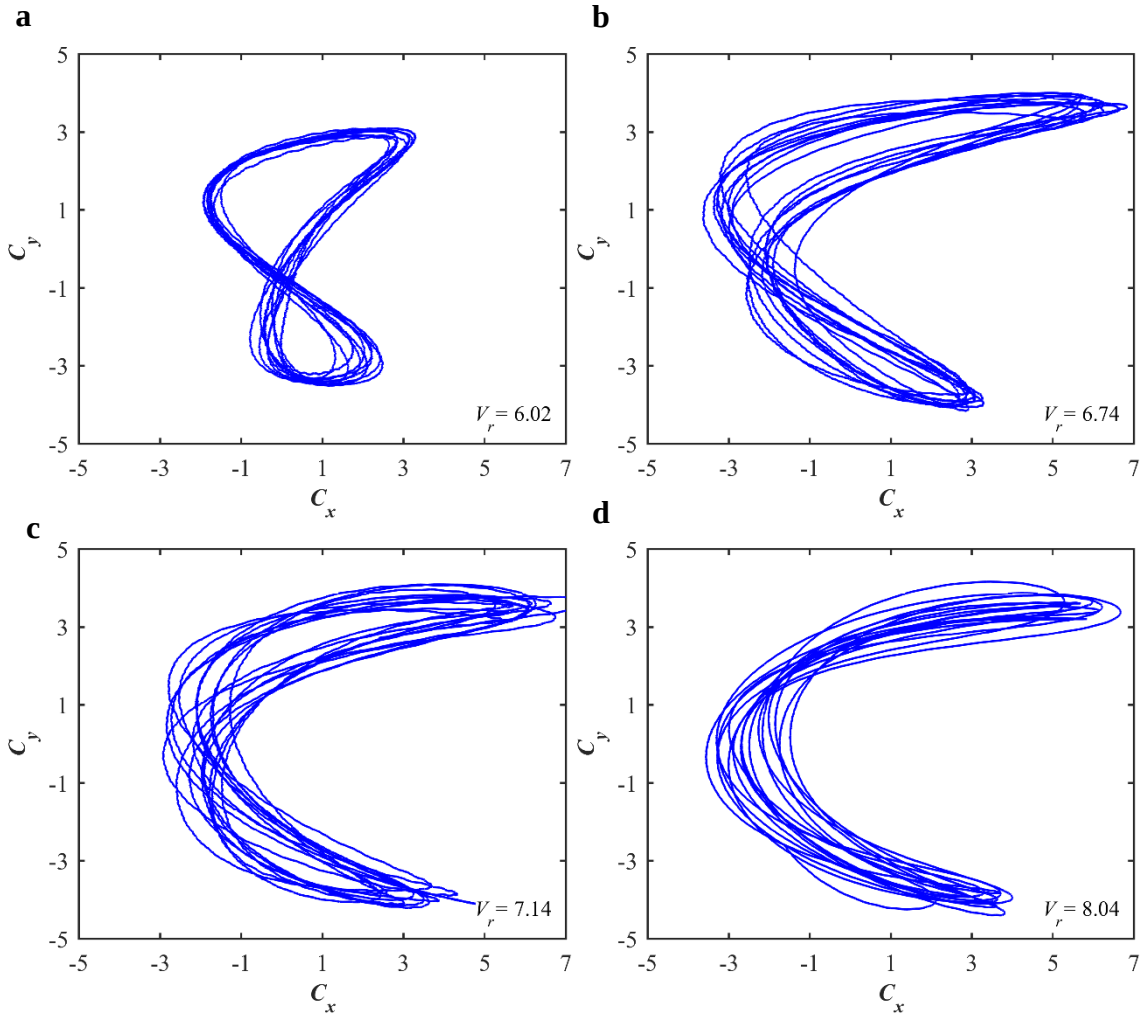

Figure 17 Sample two-dimensional trajectories of total fluid force coefficients in perpendicular flow case associated with Fig. 12: (a) V_r = 6.02, (b) V_r = 6.74, (c) V_r = 7.14 and (d) V_r = 8.04.

Highlights

- Experimental investigations of in-plane/out-of-plane VIV of curved circular cylinders are presented.
- The asymmetric effect of cylinder curvature versus the approaching flow direction is examined.
- Perpendicular (convex) flow VIV produces maximum (minimum) cross-flow/in-line responses.
- Multiple 2:1:1 resonances and cross-flow mean displacements occur in perpendicular flow cases.
- New results of VIV amplitudes and hydrodynamic coefficients of curved cylinders are provided.